D. Kluwen

Kinematics analysis of an end-effector-based orthosis for the lower limb allowing for adduction and flexion

TU Delft

Kinematics analysis of an end-effector-based orthosis for the lower limb allowing for adduction and flexion

By

Daniël Kluwen

in partial fulfilment of the requirements for the degree of

Master of Science
in Mechanical Engineering

at the Delft University of Technology,
to be defended publicly on 27-01-2022

Supervisor:	Dr. ir. L. Marchal-Crespo
Co-supervisor:	Dr. ir. H. Vallery
Thesis committee:	Dr. ir. L. Peternel

TU Delft

Preface

Even though this is not the original subject of this thesis, I'm still glad about how it turned out. Originally this thesis was supposed to be a control design thesis for the modified Lokomat. However, after assembling the modified Lokomat, there were several electrical issues, as well as missing documentation, including the kinematics, which is now the subject of this thesis. Through the work I did on the modified Lokomat I learned many different things such as making electrical schemes, how to work with programs such as EtherCAT, Matlab xPC target add-on, and LinMot talk. All in all, it was an interesting, at times, frustrating experience, that I do not regret. I hope this work can help others work with this device and that this thesis can be built upon to make controllers for the modified Lokomat.

D. Kluwen
Delft, December 2021

Contents

Abstract

Rehabilitation robotics is a rapidly growing field in the engineering industry. Due to the high repeatability of motion, high therapy costs, and lack of proper quantitative assessment of patient status and progress, rehabilitation centers could benefit from the introduction of robotics. One such device already commercially available is the bodyweight supported treadmill device Lokomat (Hocoma, Switzerland). In this thesis, the kinematics analysis for a modified Lokomat orthosis has been made and validated. These kinematics calculate the Euler angles of the orthosis hip joint as a function of eight degrees of freedom, two degrees of freedom of actuators driving the thigh, and six degrees of freedom of the orthosis pelvis body. The kinematics were validated by using a low-cost HTC Vive VR tracker system, to capture the actual angle of the orthosis hip joint. The kinematics were tested in three experiments. Firstly, the kinematics were tested by moving the orthosis around by hand, tracing the range of motion of the linear actuators. Afterward, the kinematics were validated with a person wearing the device. The first dataset has the person suspended in the air, simulating walking, whilst the final dataset has the person dragging their feet over the ground, to simulate walking. The results from the first experiment indicate that the kinematics calculation tracks the measured angles with an RMSE of less than 6% of the total range of motion. Later experiments suffered from drift in the Vive trackers, mainly in the flexion angles, worsening performance. Compensating for this drift shows the kinematics to still be similarly accurate to the first experiment.

Acknowledgments

I would like to thank my supervisor and co-supervisor, Laura Marchal-Crespo and Heike Vallery for their assistance in making this thesis.
I would like to thank Ehsan Hoseini and Andre van der Kraan for helping me repair the Lokomat and making it electrically safe.
I would like to thank Alex van den Berg for helping me with investigating the control of the Lokomat, as well as helping with setting up the Unity environment and performing the final experiments.

1 Introduction

In the US alone, each year around 795,000 people experience a stroke [1], with 80% of stroke survivors experiencing some kind of gait impairment [2]. The path to recovery is lengthy and expensive and involves many intense training sessions, both for patients and therapists.
One therapy method named Bodyweight Supported Treadmill Training (BWSTT) involves a stroke survivor walking on a treadmill whilst (part) of her/his body weight is supported. One or two therapists then assist the patient with walking by physically guiding his/her legs. This repetitive assisted motion has been shown to improve the function of the impaired limb [3]–[5]. The movement also stretches the muscles, reducing stiffness and muscle loss [5]. Research also shows that this kind of therapy fosters neuroplasticity in the central nervous system, compensating for the neuronal damage caused by the stroke [6], [7]. The issue with this kind of therapy is that it is lengthy and costly. Furthermore, conventional therapy is very taxing for therapists, leading to short training durations and, sometimes, even injuries for the therapists [8]. Lastly, the assessment of progress for clients is described qualitatively rather than quantitatively. Since this kind of rehabilitation training is highly repetitive, and because of the drawbacks mentioned above, more and more research is being done into the field of rehabilitation robotics, where the role of the therapist is (partially) taken over by a robot. Although there is conflicting evidence on whether robotic gait rehabilitation outperforms conventional therapy [9], it has often been shown that robotic gait rehabilitation can be used alongside conventional therapy for better results [10]. Robot-assisted gait rehabilitation has shown that patients' active voluntary efforts [8], [11], and making small errors [12]–[14] are considered to be important in motor learning, and thus, recovery. More research is also being done on feedback mechanisms, such as auditory [15] or visual feedback [16] to enhance the recovery process. One of these robotic gait-assisting devices, called the Lokomat (Hocoma AG, Switzerland), is a commercially available bodyweight supported treadmill device, with an integrated leg orthosis. From its inception in 1996, the Lokomat has been improved in various ways, such as VR (for the Lokomat Pro) [17]–[19] and an increased interest in more challenging recovery strategies such as visual [17] and haptic [20] error modulation.
With the rehabilitation strategies becoming increasingly sophisticated, the physical design of rehabilitation devices can become a bottleneck. Without the proper hardware, even the most advanced rehabilitation strategies cannot be used to their full potential. Common design-related challenges in orthosis-based devices such as the Lokomat are:

1. Low transparency
2. Joint misalignment
3. Limited Degrees of Freedom (DOFs)

The low "transparency" of the Lokomat has been noted before [21]. Transparency, in the broader context of physical human-robot interaction (pHRI), can be defined as the perceived quality of the desired rendered device dynamics [22]. For example, transparency can indicate the quality of virtual force rendering, by comparing the virtual dynamics to the rendered forces applied to the human. The same can be said for rendering no dynamics, i.e. putting a device in "free-motion mode", or zero-impedance mode. Low transparency leads to the participants feeling resistance when the device is in a zero-impedance mode [23]. It is often measured in the physical human-robot interaction (pHRI) forces, where having minimal interaction forces in a "free-motion" mode is considered high transparency [24]. In this free motion mode the orthosis is supposed to follow the movement of the wearer.
Joint misalignment is a common issue in exoskeletons/orthoses. Due to the deformation of both the human tissue and parts of the exoskeleton or errors in placing and attaching people

to the orthosis the axes of the joints of the human and exoskeleton can often be misaligned, causing unwanted torques.
Finally, also in the case of the Lokomat, the device can have fewer degrees of freedom in its lower limb joints than the human. This limits the range of motion, causing the motion to be unnatural in a sense. In the case of the original Lokomat, the orthosis only allows for motion within the sagittal plane in both knee and hip and does not allow pelvis rotation or translation, the latter of which has been shown to impact gait [25]. The goal of rehabilitation is to restore gait as close to normal as possible, then the device should aim to approach normal gait as closely as possible, including all DOFs of each joint.

In and around 2013-2014 at ETH Zurich, many hardware modifications were made to a Lokomat to address some of these issues. These modifications included a new 6 DOFsystem to allow the pelvis to move unconstrained, as well as a change to the hip joint and hip actuation to allow for adduction/abduction. A more detailed description of these changes will be done in Section:2 Design. The first of these changes has been researched in the Ph.D. of Dario Wyss [26], as well as a scientific paper [27]. The change to the hip joint and its actuation has been implemented but has not been researched in detail. The kinematics of the device are currently unknown and no documentation has been found to indicate the Range of Motion of the current design. This thesis will be a continuation of the work done by Wyss et al. in validating the design of the modified Lokomat, creating inverse and forward kinematics, and getting the device ready to be used in future experiments.

To achieve these goals, the thesis features the following sections:

Section 2: A short description of the modifications and their functioning/components
Section 3: The creation of forward and inverse kinematics based on said design
Section 4: A methodology for validating these kinematic calculations
Section 5: The results of the experimental validation
Section 6: Discussion of the results
Section 7: Conclusion

Also included in the Appendix are more detailed explanations of certain calculations, as well as documents important to the safety evaluation of the modifications, such as the electrical scheme of the electronics added in the modification.

2 Design

To accurately describe the kinematics of the modified Lokomat, it is important to go through the changes in the design of the device; the different actuators and sensors present in the device. In the following subsections, the modifications will be split up into these two modules:

1. Thigh actuation module
2. Compliant pelvis module

The compliant pelvis module has already been described in detail in [27] and is extensively covered in the doctoral thesis of Dario Wyss [26]. This thesis will only go into detail on the parts of the compliant pelvis module that influence the adduction/flexion system for the exoskeletal hip joint.

For each module, its main function and components will be explained, as well as how it differs from the original Lokomat, followed by a list of the actuators and sensors found in said group. These inputs and outputs of the device will then be used to determine the forward kinematics.

2.1 Thigh actuation module

The main change in the Lokomat covered in this thesis is the addition of ad/abduction to the exoskeletal hip joint, whereas the traditional Lokomat only allows for flexion/extension of the exoskeletal hip joint. The main modification that allows for this addition is the thigh actuation module. The hip joints of the original Lokomat, as of 2021, are still actuated utilizing linear drives, similar in mechanism to those found in the Lokomat's knee [28]. The linear motion is converted to a rotary motion by pushing the thigh support close to the passive revolute hip joint. To allow for this motion, the linear actuator is connected to the frame of the Lokomat, and by connection to the world, via a revolute joint in the same plane as the exoskeletal hip joint itself. This revolute exoskeletal hip joint should be in line with the human hip joint, although there is no way to guarantee this alignment, an issue common in many exoskeletons [29].
The modifications as presented in [26] have replaced the passive revolute joint with a passive 2 DOF rotational joint. This joint allows for flexion and extension, as well as limited adduction/abduction. Instead of one actuator, each hip joint now has two actuators, to allow for actuation of the additional DOF. These actuators are both rigidly attached to one another, as well as a revolute joint connected to the frame of the Lokomat, similar to the original device. The actuators and their linkages can be seen in Figure . For the sake of clarification, these actuators can be considered to be in the transverse plane (in reality this is not always the case), and the orthosis connection point connects to the posterior side of the thigh. By moving the actuators at the same speed and direction, the device can be put into pure hip flexion, for example, movement from configuration a) to configuration b) in Figure . By moving the actuators at different speeds/directions, the movement of the end effector of this linkage (which is attached to the exoskeleton thigh structure) will also have components orthogonal to the movement direction of the actuators, allowing for adduction or abduction of the hip joint - note how configuration c) has the connection to the orthosis more toward the left actuator than configuration a) and b).

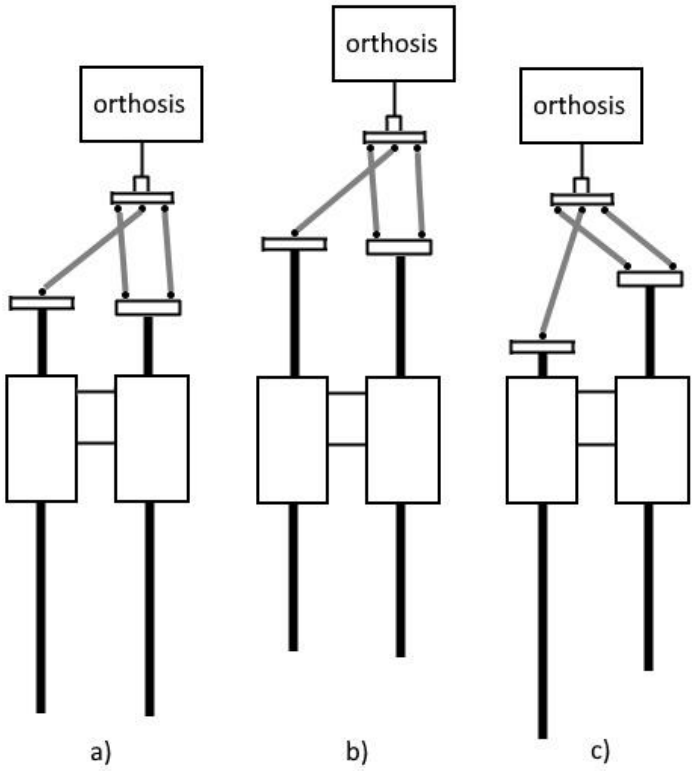

Figure 1: Various configurations of the actuators and linkages of one hip joint, with a) and b) having the actuators in parallel and c) having the actuators at an offset.

A more complete view of the mechanism can be seen in Figure 2. For the sake of simplicity, the compliant pelvis module has been left as a kinematic black box, which will be explored in the next subsection.

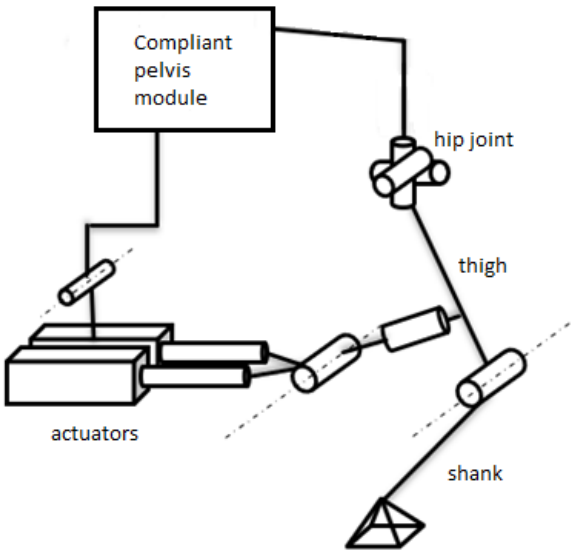

Figure 2: Joints and linkages of the thigh actuation module.

The linear actuators are LinMot P01-48x240 (LinMot, Switzerland), these are tubular electromagnetic drives. These motors are accompanied by LinMot HS01-48x250 bridge guides. The linear actuators have their own incremental encoder (resolution 0.05 mm) as well as a Micro Epsilon WPS-1250-MK46-P10 potentiometer (Micro Epsilon, Germany), to calibrate the linear motors and have redundancy in case either sensor fails. The potentiometer and the internal encoder of the actuator are the only sensors for the module.

The main input to the module is the extension of the LinMot, although the max speed and acceleration to achieve this position can be set and changed as well. For this thesis, only the position will be considered, with other motor input parameters considered static.

2.2 Compliant pelvis module

The main focus of the modifications was not only on the additional DOF for the hip joint but also on additional DOFs for the pelvis. The original Lokomat only has one passive degree of freedom for the pelvis, namely the parallelogram structure that allows for vertical movement [4]. Limiting the other 5 degrees of freedom has been found to negatively affect gait characteristics [25]. The goal of Wyss et al. [26], [27] was to expand this to the full 6 DOF, 5 passive DOFs, and one active DOF. The lateral movement of the pelvis is actuated in this design, whilst the other degrees of freedom are passive. These passive DOFs are supported by springs to still aid the wearer of the exoskeleton, see Figure .

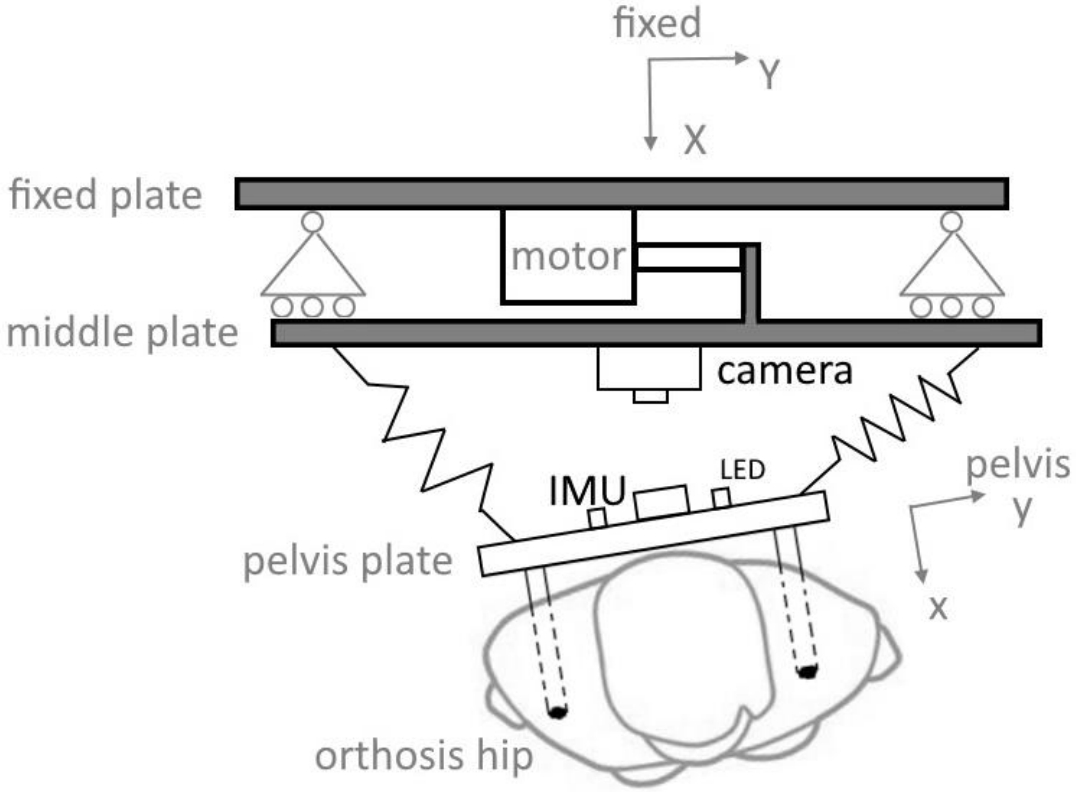

Figure 3: Top view of the compliant pelvis module, with actuators and sensors.

This modification uses series elastic actuation (SEA), as the springs are interjected between the actuator and load. The wearer is attached to the pelvis plate via clamps, which due to the application of SEA, has 6 DOF. The fixed plate is attached to the rigid frame of the modified Lokomat and can be seen as a connection to the world. The motor, another LinMot motor just like the thigh actuation module, actuates the lateral movement of the pelvis by moving the middle plate, which is connected to the pelvis plate via the springs. Important to note is that the entire thigh actuation module is attached to the middle plate as well so that it moves with the lateral pelvis movement to prevent unwanted adduction/abduction of the hip due to latera pelvis movement. For more information on the system and how the springs are tuned, see [26], [27].

What is important for the calculation of the adduction/abduction angles is the location of the exoskeletal hip joint in relation to the thigh actuation module, to complete the kinematic chain. This hip joint is attached to the pelvis plate of the compliant pelvis module. This attachment is rigid, although it can be adjusted in the anatomical longitudinal axis, to account

for anatomical differences between users. To know the location of the exoskeletal hip joint, the position and orientation of the pelvis plate must be known. Fortunately, Wyss et al. [26], [27] required the same information to determine the assistive forces provided by the springs. The sensor system put in place uses a camera system (PixArt Imaging Inc., Argentina) with an infrared filter, accompanied by four infrared Light-Emitting Diodes (LEDs) attached to the pelvis plate. The camera translates the position of the four LEDs in pixels to the location and orientation of the pelvis plate. Also included is an Inertial Measurement Unit (IMU) (MPU9250, Invensense, San Jose, USA), to record the movements of the pelvis, which can also be doubly integrated to receive an estimate of the position and orientation of the pelvis plate. These signals are combined through the use of a Kalman filter to determine all 6 degrees of freedom for the pelvis plate.

2.3 Full system

Combining both the compliant pelvis module as well as the thigh actuation module, the system looks as follows (Figure):

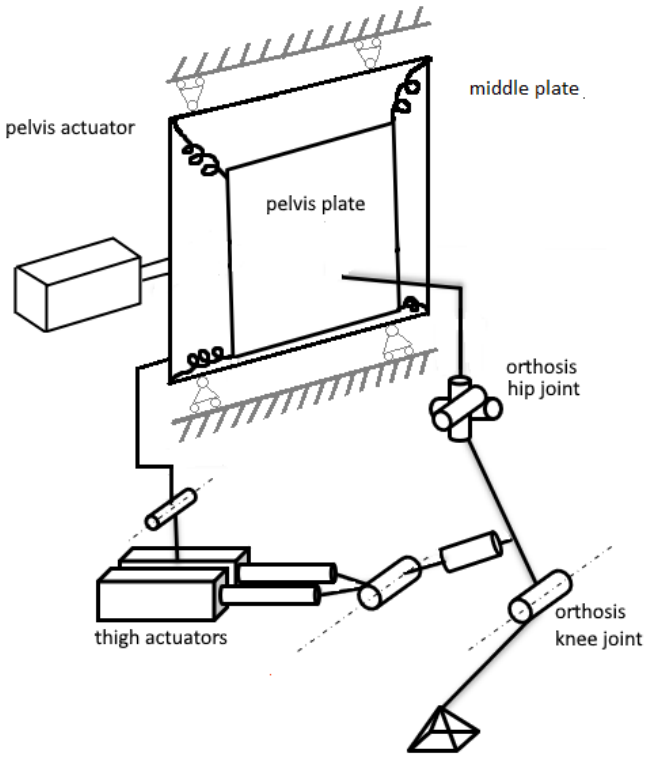

Figure 4: Schematic of the orthosis of a single leg and hip assembly of the modified Lokomat.

In Figure , the rest of the Lokomat is represented as the ground. The pelvis actuator creates lateral movement of the pelvis by actuating the middle plate. As the thigh actuators are attached to this middle plate, they too will move laterally. As the orientation and position of the pelvis plate are measured from the middle plate (**Fout! Verwijzingsbron niet gevonden.**), it is possible to close the kinematic chain without the inclusion of the pelvis motor. The kinematic chain would start at the middle plate, from where we can find the position of the pelvis plate through the camera and IMU, from where the orthosis hip joint can be found, followed by the thigh actuation and finally closing the loop at the middle plate. Hence only the following sensors and actuators of the orthosis and pelvis actuation system are relevant for the calculation of the orthosis hip angles:

sensors			
sensor	measured parameter	unit	amount
LinMot encoder	extension linear motor	*m*	2 (per leg)
Potentiometer	extension linear motor	*m*	2 (per leg)
Camera	orientation and position pelvis plate	*m, degrees*	1
IMU	Orientation and position pelvis plate	*m, degrees*	1
actuators			
actuator	actuated parameter	unit	amount
LinMot motor	extension linear motor	*m*	2 (per leg)

Table 1: Actuators and sensors involved in the calculation of the orthosis hip angles.

3 Kinematics calculation

Now that the design of the modified Lokomat has been explained, and the relevant available inputs and outputs have been specified, the kinematics calculation can begin. To repeat, the goal of the forward kinematics calculation is to find a way to calculate the exoskeleton hip angles - i.e., flexion/extension, and adduction/abduction- using the sensor values from Table 1 and vice versa for the inverse kinematics.

To start, a check of the degrees of freedom of the device will be done, to check whether the device has as many DOFs as stated in section 2. The next step will be to calculate the forward dynamics using the eight measured coordinates, followed by the inverse dynamics.

3.1 Degrees of freedom of the mechanism

As mentioned in the design phase, the modification to this Lokomat should result in a total of 12 degrees of freedom. These degrees of freedom are:

- 6 DOFs in the pelvis
- 4 DOFs for the hip joints (hip adduction and flexion for each leg)
- 2 DOFs in the knees (knee flexion for each leg)

For this thesis specifically, the interest lies in the 2 DOFs for each hip joint. Due to the symmetry in the design, it is possible to disregard one leg for the kinematic calculations. Also as explained in section 2.3, the kinematic chain from hip joint to thigh actuators can be closed without the inclusion of the lateral pelvis actuator. So the remaining system considered in this thesis should have a total of 8 DOF, 6 for the pelvis plate, and 2 for the single exoskeletal hip joint.
One way of checking the degrees of freedom of a system is to express the system in generalized coordinates. The amount of independent generalized coordinates needed to fully describe the system is equal to the degrees of freedom of that system. Besides describing the system in just the independent generalized coordinates, one can also add more coordinates to make the description easier, as long as the dependency to the other coordinates is described in the form of a constraint. Using this method, one can also check the degrees of freedom by counting the number of generalized coordinates, some independent, some dependent on one another, and subtracting the number of constraint equations. The latter method will be deployed in this case as the system is quite complex. Figure shows all generalized coordinates chosen for this DOF calculation, apart from the coordinates around the thigh actuators, in particular the path from joint **O** to joint **D**. These coordinates are shown in Figure 6. Note that Figure 6 is a 2-dimensional representation. This is allowed as all the hinges are oriented in the same way, in the same plane in which the system is also actuated.

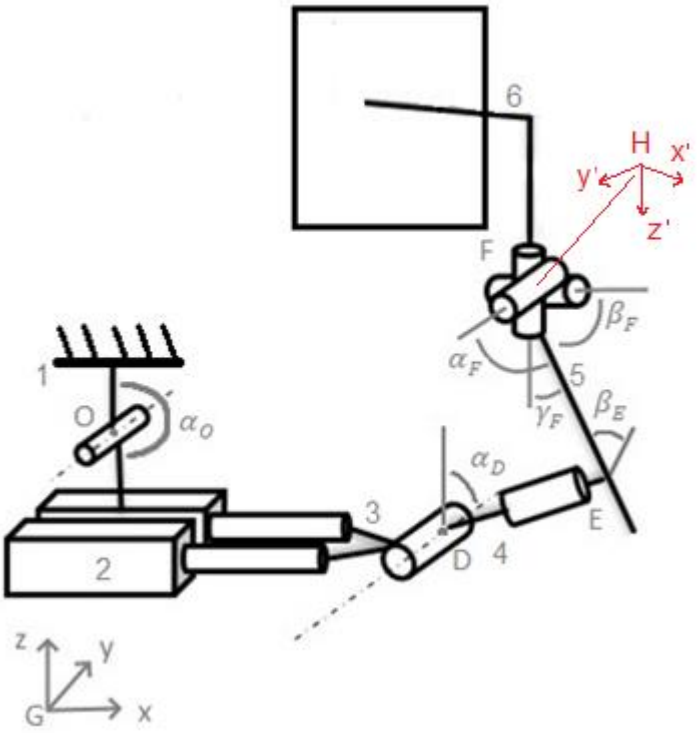

Figure 5: Drawing of the thigh actuation and partial pelvis module with generalized coordinates. α_O represents the angle between body 1 and 2 around hinge O, α_D the angle between body 4 and the global z-axis, around joint D, β_E the angle between body 4 and 5 around joint E, and α_F , β_F , γ_F the angles between the axes of frame H (attached to body 6) and body 5.

The goal of this calculation will be to know the 6 DOFs of all 6 bodies as presented in Figure 5, starting at the ground body, body 1. Body 1 is connected to body 2 by a single DOF hinge joint at **O**. Body 2 consists of the two static parts of the linear motors, which are rigidly connected to one another. By introducing α_O as the angle between body 1 and 2, around the axis of joint **O**, body 2 can now be fully described kinematically. As said, previously, everything between body 2 and joint **D** can be considered a planar mechanism, whose plane is tilted around the global y-axis with angle α_O. Continuing at joint **D**, body 4 can be fully described using the angle α_D, as this joint is another hinge joint. Using β_E the same can be done for the thigh orthosis, body 5. Joint **F** is a ball and socket joint with 3 DOF, hence 3 angles are required to fully express body 6 in relation to body 5. In this case, the angles were chosen to be measured from body 5 to a body-fixed frame (H) attached to body 6. So far 6 generalized coordinates have been used, with zero constraints:

1. Angle α_O , the angle between body 1 and body 2
2. Angle α_D, the angle between body 4 and the global z-axis
3. Angle β_E, the angle between body 4 and 5
4. Angle α_F, one of the Euler angles between body 6 and body 5
5. Angle β_F , one of the Euler angles between body 6 and body 5
6. Angle γ_F, one of the Euler angles between body 6 and body 5

Next up is the planar mechanism between point **O** and joint **D**, which can be seen in Figure 6.

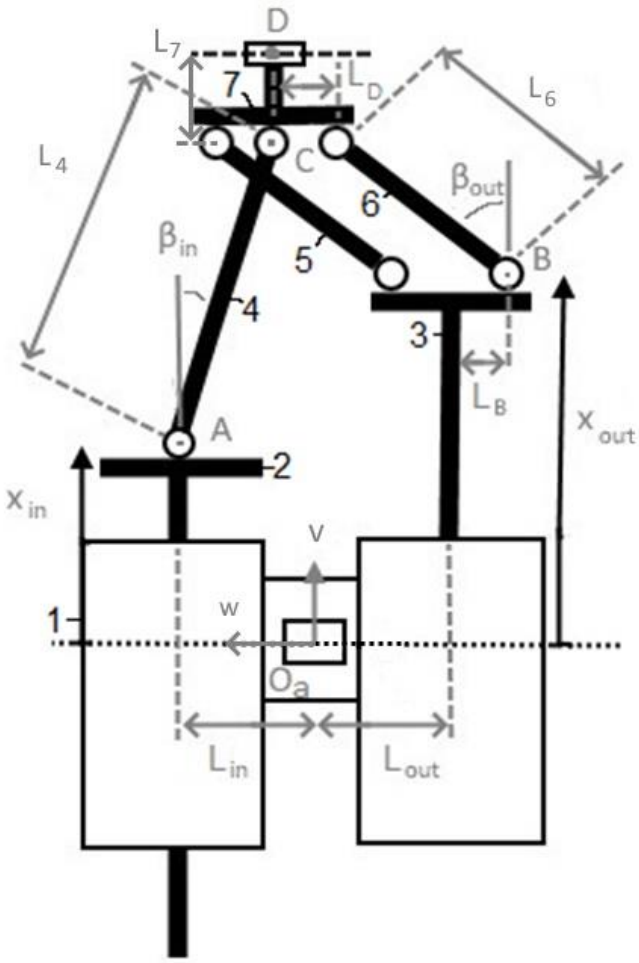

Figure 6: Two-dimensional drawing of the thigh actuation linkages. The frame O_a is attached to body 1 and centered at point O, with axes v and w. x_{in} and x_{out} represent the distance from point O_a to point A and B respectively, along the v axis. L_{in} and L_{out} are the distance from point O_a to point A and B respectively, along the w axis. β_{in} and β_{out} are the angles of linkage 4 and 6 to the v axis and L_4 and L_6 are their lengths. L_D is the distance between the outer actuator and point D along the w axis. L_7 is the distance between point D and point C and L_B is the distance between the symmetry axis of body 3 and point B.

For the linear actuators, we start at point **O**, which corresponds to joint **O** in Figure . Though this joint is drawn above the linear actuators in Figure , it is located at the centerline of all bodies in Figure 6. Starting from point **O**, one can reach joint **D** in two ways, tracing the linkages from the inner or outer actuator. Taking the inner actuator, we can reach point **C** using generalized coordinates x_{in}, which contains the extension of the linear actuator, as well as angle β_{in}. The linear actuators used in this assembly have guides, meaning they can be treated as prismatic sliders with only one DOF, which can be described by the generalized coordinates x_{in} and x_{out}. The orientation and position of linkage 4 can be described just by using the generalized coordinate β_{in}, at which point we know the position of joint **C**, attached to body 7.

$$w_C = -L_{in} + L_4 \sin(\beta_{in}) \tag{1}$$

$$v_c = x_{in} + L_4 \cos(\beta_{in}) \tag{2}$$

The orientation of body 7 is unknown when only considering the inside actuator linkages, however, note that the four-bar linkage created in the outer actuator linkages, by body 3, 5,6, and 7 is a parallelogram. This means that body 7 will always be oriented with its long side along the w axis. For the linkages connected to the outer actuators, all DOFs can be

expressed in the same way as the inner actuators, considering that angle β_{out} applies to both linkage 5 and 6, due to the parallelogram they form. With the position of point **C** and the orientation of body 7 known, the assembly has been fully described.

$$w_D = w_C \tag{3}$$

$$v_D = v_C + L_7 \tag{4}$$

There are two constraints present in this formulation, namely that point **C** has to be in the same location, whether you calculate its position from the inner or outer actuators. This results in two unique constraints, one for the v and a second for the w coordinate.

In summation, all bodies in this system can be fully described using 4 generalized coordinates; x_{in},x_{out}, β_{in} and β_{out}. These generalized coordinates are subject to 2 constraints, the v and w coordinates of point C are the same coming from the inner or outer actuator. Counting up all the generalized coordinates from Figure and Figure 6, there are 10 generalized coordinates used to fully describe the system, subject to 2 constraints, leaving the number of DOFs to 8, as expected.

3.2 Forward kinematics

Now that it has been shown that the kinematics can be described using 8 independent generalized coordinates, it is possible to express the kinematics in terms of the sensed parameters from Table 1. The generalized coordinates used in the DOF calculation are chosen for convenience, but they are not easily transformed into coordinates that match the sensors present in the device. Figure is a drawing of the modified Lokomat with the sensed generalized coordinates:

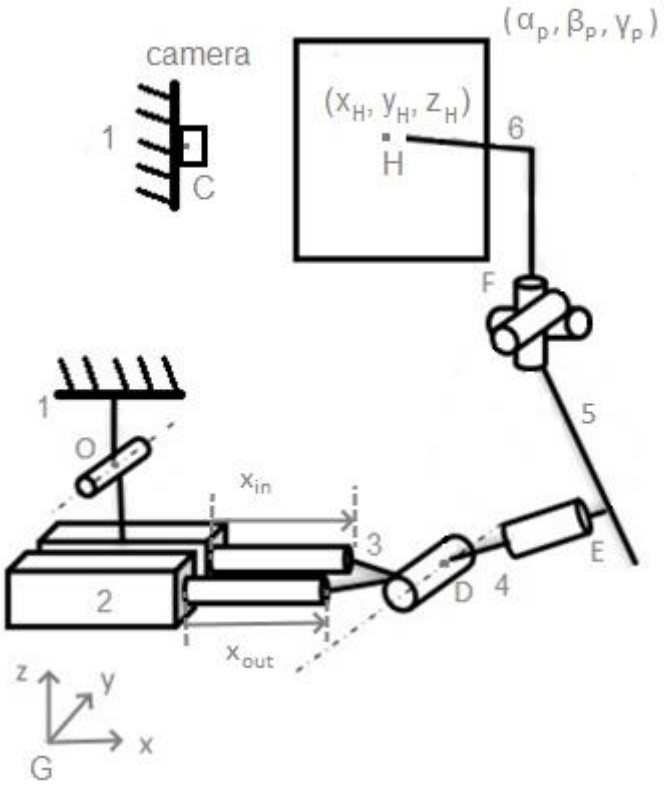

Figure 7: Drawing of the modified Lokomat, using the sensed values as generalized coordinates. The coordinates include the position of the pelvis plate (x_H, y_H, z_H) and its orientation in relation to the fixed ground frame). The orientation is expressed in Euler angles α_p, β_p and γ_p. The other two coordinates are the extension of the inner and outer actuators, x_{in} and x_{out}, respectively.

With the new sensed generalized coordinates, the orientation and position of the pelvis plate (body 6) is fully known in relation to the ground by the camera at **C** and the IMU at **H**. By extension, the position of ball and socket joint **F**, the exoskeletal hip joint, is also known as it is rigidly attached to body 6. As seen in Figure 6, the thigh actuation linkages (the bodies from joint **O** to joint **D**), require four generalized coordinates and 2 constraints to be described, hence these bodies can be described using two independent generalized coordinates, in this case, x_{in} and x_{out}. Removing the generalized coordinates β_{in} and β_{out} from Figure 6, the orientations of linkage 4, 5, and 6 become unknown. This unknown orientation can be expressed by drawing a circle around the corresponding joint, where the circle represents the potential positions of the endpoint of the linkage for all orientations. In Figure these circles are drawn for the inner and outer linkages.

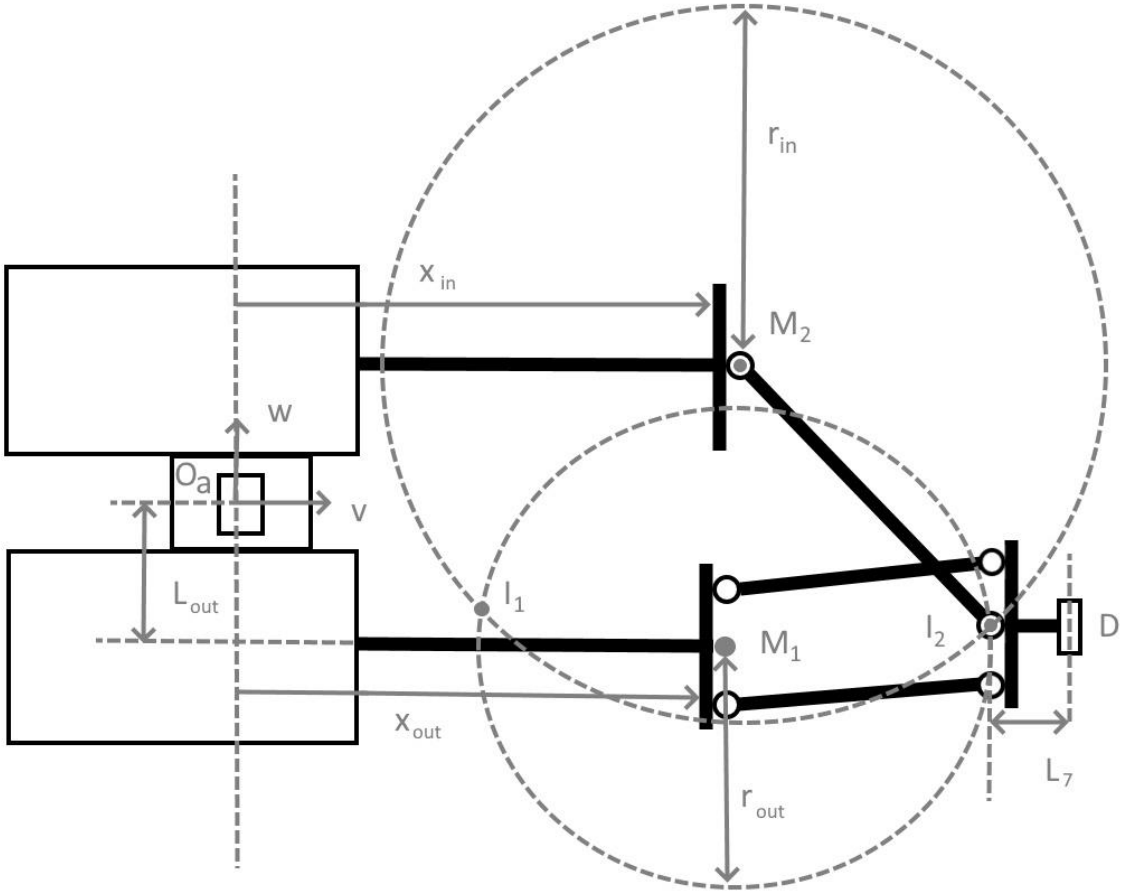

Figure 8: Two-dimensional drawing of the thigh actuation linkages. The frame O_a is attached to body 1 and centered at point O_a, with axes v and w . The x_{in} and x_{out} represent the extension of the actuators and are the two independent generalized coordinates. L_{out} isthe distance from O_a to the actuator slider in the wdirection. The circles, with middle points M_1 and M_2 and radii, r_{in}, and r_{out} represent the range of motion of the endpoint of the inner and outer linkages respectively. The circles intersect at points I_1 and I_2. L_7 is the distance from point I_2 to joint D.

The endpoints of both inner and outer linkages are connected, so the only two places where the linkages can be connected and do not break constraints, are the two intersection points of the circles, $\mathbf{I_1}$ and $\mathbf{I_2}$. Finding the intersection of two circles in cartesian space can be done using the equations of a geometric proof, in this case, taken from [30], see Appendix A. In Appendix A, the circle intersection calculation is first explained in abstract, after which it is applied to the situation from Figure 8. The input for this calculation is the coordinates of the center of both circles ($\mathbf{M_1}$ and $\mathbf{M_2}$ in this case) and the radius of both circles (r_{out} and r_{in}). The output is the coordinates of both intersection points $\mathbf{I_1}$ and $\mathbf{I_2}$, which can be used to determine

the coordinate of point **D** and the orientation of the body to which point **D** is attached. Although $\mathbf{I_1}$ is a solution to the intersection calculation, it can be seen that it is not physically possible for the linkages to be in this configuration, due to a collision between the slider of the actuator and the linkages, hence $\mathbf{I_2}$ is the actual intersection point. The location of point **D** can be found from point $\mathbf{I_2}$ by adding L_7 to the *v* coordinate of point $\mathbf{I_2}$ since the body that **D** is attached to is always orientated the same way due to the parallelogram structure in the outer linkages. This parallelogram locks the rotation of the body that **D** is attached to, meaning that a vector from $\mathbf{I_2}$ to **D** will always be along the *v* axis purely.

The vector $\overrightarrow{\boldsymbol{OD}}$ is now known in the body-fixed frame, but the location of **D** is not yet certain in the global frame G (see Figure), due to the unknown angle α_O around joint **O**, see Figure 5. Since joint **O** is another hinge joint, it is possible to once again use a circle to describe the possible locations of point **D** in the global frame **G**, see Figure (left).

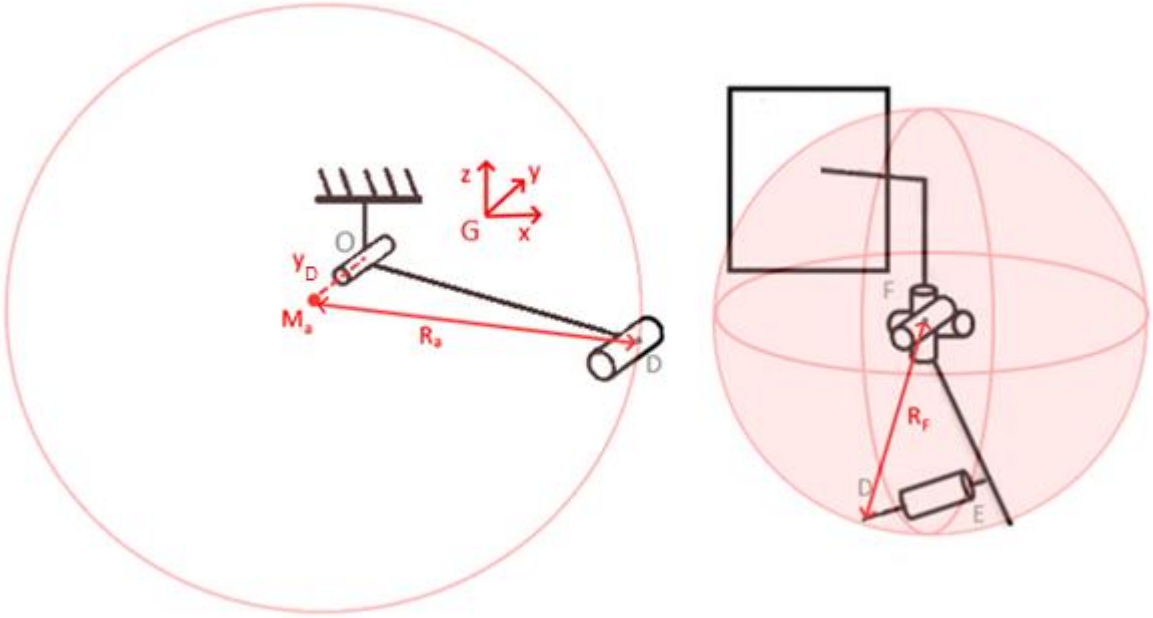

Figure 9: Potential locations of point D, expressed around joint O (left) and joint F (right). With M_a and R_a the center point and radius of the circle around the actuators. y_D is the distance between M_a and R_a in the global y-axis. R_F is the radius of the sphere with center point F.

In the global frame (G), the circle is in the xz plane, as joint **O** will always have a rotation around the y axis. The plane in which the circle is located will be offset from point **O** at a distance of y_D along the global y-axis, where y_D is equal to the y coordinate of point **D** from Figure . The radius of the circle will be R_a, the *v* coordinate of point **D** from Figure .

$$R_a = v_D \tag{5}$$

$$y_D = w_D \tag{6}$$

The range of motion of the thigh linkage can be described in a similar fashion, although the resulting geometry will be a sphere rather than a circle, as join F is a ball and socket joint. Rotation around joint **E** does not change the location of point **D**, it would only change the orientation of the body to which point D is attached., hence it does not influence the shape of the sphere. The radius of the sphere, R_f will be distance between joint **F** and point **D**.

The actual location of point **D** can again be found through the intersection points of these two geometries. There will be two intersection points between a circle and a sphere. Furthermore, the problem can be simplified by considering that the sphere can only intersect

the circle in the plane of the circle, in this case, a plane parallel to the xz plane of the global coordinates, with offset y_D from joint **O**, see Figure .

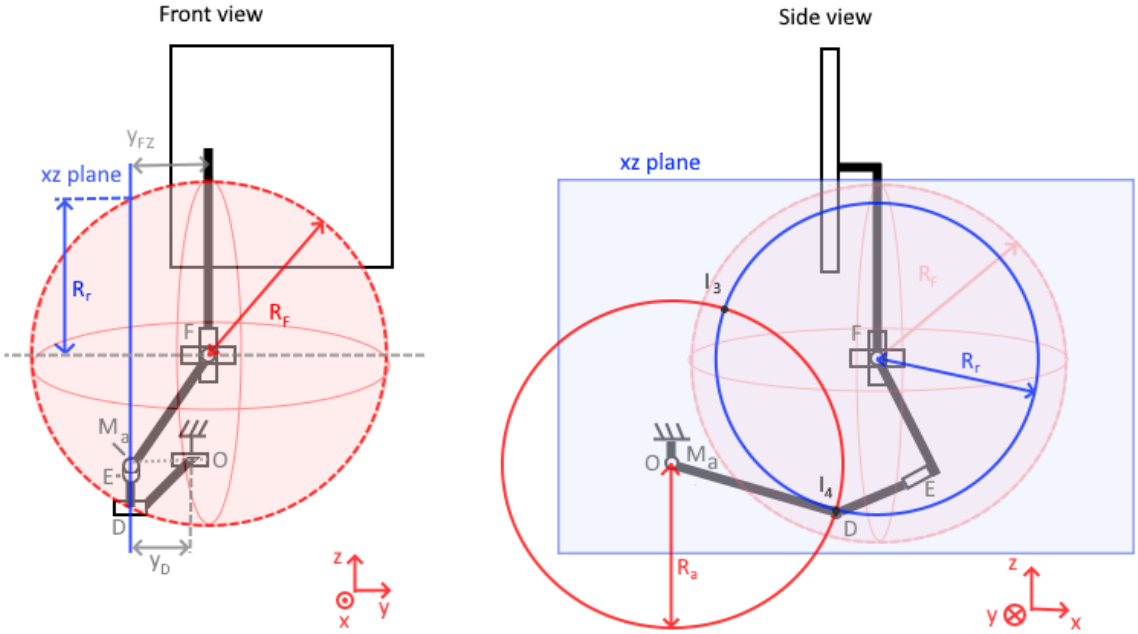

Figure 10: Front view (left) and side view (right) of the intersecting geometries used to determine the location of point D. The circle with projected center M_a and radius R_a is located in the plane parallel to the xz plane, with offset (blue) y_D from point O. The sphere with center F and radius R_f intersects the aforementioned circle at points I_3 and I_4. The section of the sphere contained in the offset plane parallel to the xz plane is a circle with projected center F and radius R_r. the distance between joint F and the offset xz plane is y_{FZ}.

The distance between joint **O** and **F** is known since the camera measuring the pelvis plate is also attached to the ground, like joint **O**. From the camera, the pelvis plate location and orientation are known, leading to the location of joint **F**. Using the y coordinate of the vector $\overrightarrow{\boldsymbol{OF}}$ and y_D one can calculate the distance of joint **F** to the xz plane (y_{FZ}). The section of the sphere in the offset xz plane is a circle, with a reduced radius R_r. Calculating R_r can be done using the Pythagorean theorem on the right triangle created by the black dashed line in Figure :

$$R_r = \sqrt{(R_F)^2 - (y_{FZ})^2} \tag{7}$$

With R_F, the circle of the sphere is defined as:

$$R_F = \left\|\overrightarrow{\boldsymbol{FD}}\right\| \tag{8}$$

All components for the intersection calculation are now known:

- Radius R_a is the x coordinate of the vector $\overrightarrow{\boldsymbol{OD}}$
- The coordinates of the center point of the circle are the (x,z) coordinates of point **O**
- The radius of the second circle is R_r, the derivation can be seen above
- The coordinates of the center point of the second circle are the (x,z) coordinates of point **F**

With these values, the intersection points $\mathbf{I_3}$ and $\mathbf{I_4}$ can be calculated. Whether the physical joint **D** is in $\mathbf{I_3}$ or in $\mathbf{I_4}$ can be checked via the z-coordinate of both points. If the z-coordinate of one of the intersection points is too high, linkage **OD** will hit the ground body above **O**. In this case $\mathbf{I_4}$ would be selected. Knowing the coordinates of point **D**, all bodies have now been described kinematically, the only thing remaining is the calculation of the orthosis hip joint angles.

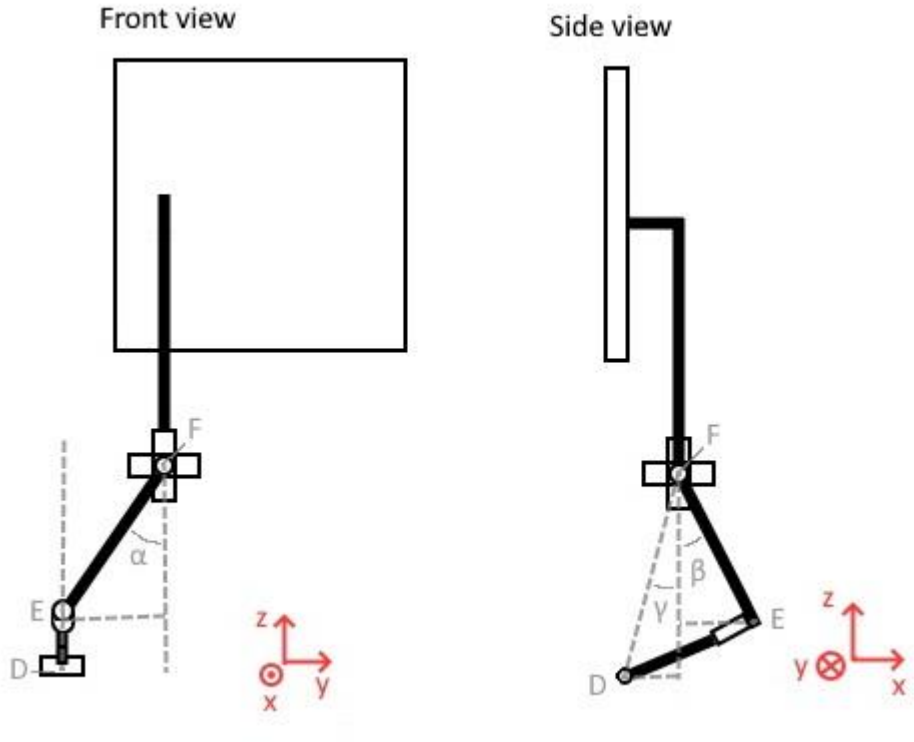

Figure 11: flexion angle β and adduction angle α assuming a neutral pelvis.

With the assumption that the pelvis plate remains in a neutral position, coordinates of point **D** and **F** in the global frame, the adduction angle α, and the flexion angle β can be calculated.

$$\alpha = \sin^{-1}\left(\frac{y_F - y_E}{\|\boldsymbol{FE}\|}\right) \tag{9}$$

With y_F and y_E the y coordinates of points **F** and **E** respectively, and $\|\boldsymbol{FE}\|$ the magnitude of the vector from point **E** to point **F**. Due to the four-bar linkage attached to joint **D**, joint **E** and **D** are always at the same global y coordinate:

$$y_E = y_D$$

Then finally, the flexion with neutral pelvis β can be calculated using:

$$\beta = \tan^{-1}\left(\frac{\|\boldsymbol{FE}\|}{\|\boldsymbol{DE}\|}\right) - \sin^{-1}\left(\frac{x_F - x_D}{\|\boldsymbol{FD}\|}\right) \tag{10}$$

With $\|\boldsymbol{FE}\|$ and $\|\boldsymbol{DE}\|$ the magnitude of vectors between **F** and **E** and **D** and **E** respectively. x_F and x_D the x coordinates of points F and D respectively, and $\|\boldsymbol{FE}\|$ the magnitude of the vector from point **E** to point **F**. This calculation relies on the right triangle formed by points **D**, **E** and **F**.As previously mentioned, these angles are not the true exoskeletal hip joint angles, as they assume a neutral pelvis position. To incorporate the hip angles, it is more manageable to calculate the Euler angles between a local frame of the pelvis and thigh. The angles described above can be used to create the thigh axes. The pelvis axes can be made using the recorded Euler angles of the pelvis plate.
To define said angles, the anatomical conventions for joint coordinate systems from Sharp et al. [31] will be adapted to fit the orthosis. This convention places two joint coordinate systems on the pelvis and thigh respectively and defines the joint angles as the Euler angles between

these two coordinate systems. The conventions and their adaptation to the orthosis can be seen in Figure 12.

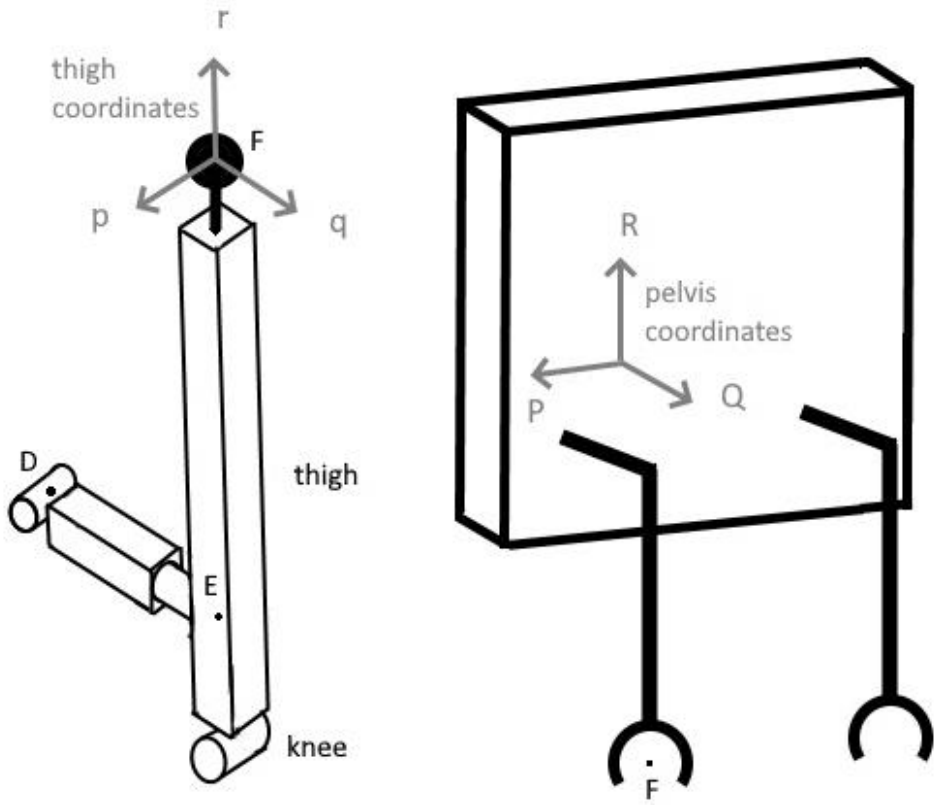

Figure 12: Conventions for the calculation of hip angles for human gait motion analysis, taken from [31]**, adapted to the modified Lokomat orthosis. P, Q, and R are the axes of the pelvis coordinate system, whilst p, q, and r are the axes of the thigh coordinate system.**

Starting with the pelvis coordinate system:

1. The P-axis can be found by taking a unit vector parallel to the bottom of the pelvis plate, or a unit vector from the left to right hip joint.
2. The R-axis can be found as a unit vector orthogonal to the Z-axis, in the plane of the anterior side of the pelvis plate, pointing cranially.
3. The Q-axis can be found as a unit vector orthogonal to the Z and Y axis, pointing to the anterior side

The thigh coordinate system is defined as:

1. The r-axis is a unit vector following the exoskeletal thigh beam, in this case, it can be expressed as $\overrightarrow{EF}$ normalized
2. The q-axis can be derived by normalizing $\overrightarrow{DE}$**.** This vector is orthogonal to the y axis since the linkage between **E** and **D** is attached at a 90-degree angle to the thigh linkage
3. The p axis can be found orthogonal to the x and y-axis, pointing to the anterior side

The coordinate system of the pelvis plate made by Wyss et al. [27], used to calculate the Euler angles of the pelvis plate in relation to the camera coordinate system, is not the same as the one defined above, and is rotated -90 degrees around the X-axis. With these coordinate systems, Euler angles regarding the X-x axes are internal/external rotation, angles regarding the Z-z axes represent abduction/adduction, and rotations regarding the Y-y axes represent flexion/extension.

3.3 Inverse kinematics

For the inverse kinematics, the goal is to calculate the extension of the inner and outer linear actuators, x_{in} and x_{out}, as a function of the desired ad/abduction and flexion/extension, taking into account the orientation of the pelvis plate. Compared to the forward kinematics this is much simpler.

Starting from the pelvis plate, of which the orientation and position in the global frame are known, the position of joint **F** can be calculated. From joint **F**, the position and orientation of the thigh linkage are known, by using the two input angles of adduction and flexion, as well as the previously mentioned constraint that $y_E = y_D$ in the global frame (as the axis of joint **D** is always aligned with the global y-axis due to the parallelogram structure). From the location of point **D** and point **O**, it is possible to determine the angle β_O, see Figure 13.Figure

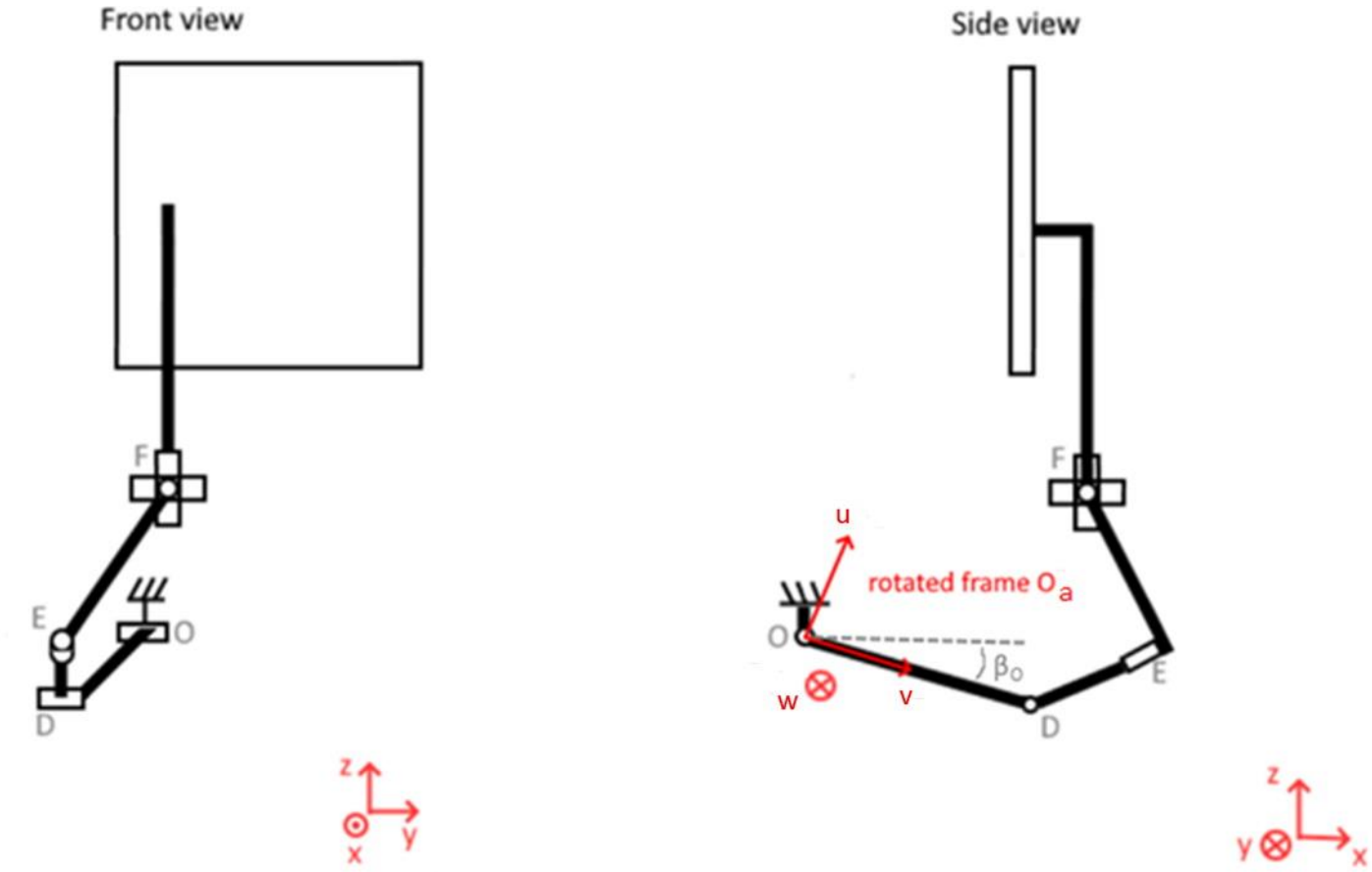

Figure 13: front and side view of the modified Lokomat, with angle β_O between the global y axis and linkage OD and rotated frame O_a with axes u, v, and w.

Calculating β_O can be done using the following equation:

$$\beta_O = \tan^{-1}\left(\frac{z_O - z_D}{x_D - x_O}\right) \tag{11}$$

With β_O it is possible to create the frame O_a, with origin in point **O**. The benefit of this frame is that it turns the actuator assembly and its linkages into a 2-D problem, as there is no variation in the u axis in the linkages spanning **O** to **D**. Inside this frame O_a, the required extension of the inner and outer actuator can be calculated using the intersection of a line and a circle. The circle represents the unknown orientation of the inner or outer linkage, whilst the line represents the extension of the inner and outer actuator, see Figure 14.

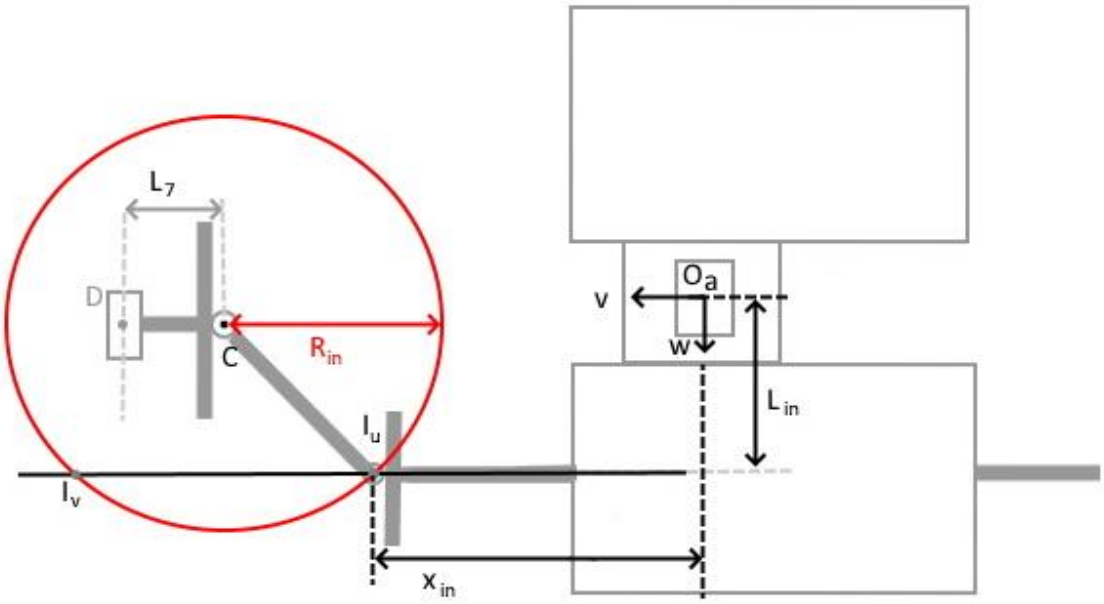

Figure 14: Planar geometries required to calculate the extension of the inner actuator. With L_C the distance between joint D and C is in the direction of the v axis. C is the center point of the red circle with radius R_{in}. This circle intersects the black line representing the extension path of the actuator in points I_V and I_u. x_{in} is the current extension of the actuator along the v-axis, this extension is measured from v = 0 to the joint at the end of the actuator, at a distance of L_{in} along the w-axis from origin O_a.

Point **C** can be found by subtracting L_{DC} from the w value of point **D**, their v values are the same. Around point **C**, the ROM of the inner and outer linkage can again be described as a circle in this case the circle in red, with mathematical description:

$$(v - v_C)^2 + (w - w_C)^2 = (R_{in})^2 \tag{12}$$

With v and w as variables, v_C and w_C the coordinate of points **C** and R_{in}, the radius of the inner linkage. The solid black line intersecting the circle represents the ROM of the slider of the linear actuator, with mathematical description:

$$w = L_{in} \tag{13}$$

The intersections of these two ROMs represent the configurations that do not break the constraints of either linkage or slider, in this case, $\mathbf{I_u}$ and $\mathbf{I_v}$. The values of these intersection points can be calculated by substituting the line equation into the circle equation and solving for v. This will turn into a quadratic equation that can be solved using the quadratic formula. Again it is possible to exclude one of the intersection points, $\mathbf{I_v}$ in this case, as it would case a collision in the linkages, mathematically this constraint can be represented as:

$$v_I \leq v_C \tag{14}$$

With v_I the v coordinate of an intersection point and v_C the v coordinate of point **C**. This same process can be done for the outer linkages as well. From the intersection point $\mathbf{I_c}$, the actuator extension x_{in} can be found by removing L_{ax} from the v coordinate of $\mathbf{I_u}$ (see Figure 14). This same calculation can be repeated for the outer linkages to find x_{out}.
With the values of x_{in} and x_{out} found, as a function of the abduction and flexion angles, as well as the position and orientation of the pelvis plate, the inverse kinematics are complete.

4 Experimental procedure

Now that the kinematics of the Lokomat have been described, they have to be validated through experimentation. For the validation process, the 8 inputs to the forward kinematics, as described in section 2.1, will be recorded. Using these recorded sensor values, the abduction and flexion angles can be calculated. These calculated values can then be validated against an external measurement of the same angles. In this case, the external measurement was done using the HTC Vive Pro (HTC, Taiwan) Virtual Reality (VR) system, which has a camera system with motion trackers. This validation process was done for three separate experiments. The first experiment aims to explore the range of motion of the device, by moving the thigh around by hand. The second and third experiments will have a subject inside of the Lokomat, simulating walking. This section will feature:

1. The recorded Lokomat variables and their calibration
2. The recorded HTC Vive variables
3. The procedure for the three experiments that were performed

After the experimental procedure has been detailed, the next section will cover the results of the experiments.

4.1 Lokomat recording and calibration

The kinematics calculation requires 8 inputs, which in this case are:

1. The extension of the inner and outer linear actuator, x_{in} and x_{out}
2. The position of the pelvis plate in relation to the middle plate (**Fout! Verwijzingsbron niet gevonden.**), x_P , y_p and z_p
3. The orientation of the pelvis plate in relation to the middle plate, Euler angles ϕ_p, θ_p and ψ_p

However, inside the modified Lokomat, there are several ways of measuring these values. For the extension of the inner and outer actuator, there are two choices: using the internal encoder of the LinMot linear motor or using the linear string potentiometer, which is normally used to calibrate the encoder. For safety reasons, it was chosen to not power the LinMot motors to prevent any dangerous movements from occurring. The only downside of the potentiometer compared to the encoder is the dynamics of the string, which should not be an issue considering the low frequency of the motions.

For the six degrees of freedom of the pelvis plate, there is the previously mentioned infrared camera system, as well as an IMU, both capable of measuring the six DOF of the pelvis plate. The camera system records the back of the pelvis plate, on which four infrared LEDs are placed, at a sampling rate of 100 Hz with 1024x1024 resolution. The pixels on which the LEDs are in the camera's images can then be transformed into a rough estimate of the position and orientation of the pelvis plate in relation to the camera, which is attached to the middle plate. The downsides to this approach are that the camera can suffer interference from other sources of infrared light, such as the infrared camera system of the HTC Vive. Furthermore, the field of view of the camera is limited, and it is possible for the LEDs to leave the field of view, causing a loss of data. These two factors make relying on the camera alone not feasible since datasets often have missing data. The second sensor, the IMU, measures the acceleration and angular velocity of the pelvis plate, at a rate of 500Hz. Using time integration, these signals can be turned into the position and orientation of the pelvis plate. However, drift is a major issue in this approach. Datasets that go on for over five seconds or more, will feature significant drift. In the past, the camera data and IMU data were combined

using a Kalman filter, where the drift of the IMU data would periodically be corrected by the camera data. This Kalman filter was unfortunately not present in the control setup of the Lokomat, so only the separate IMU and camera data are available. Neither of these sensors is reliable enough to use for the experiment, hence it was chosen to disregard these in favor of the HTC Vive tracker system, which will be discussed in the next subsection.

4.2 HTC Vive Pro recording and calibration

The HTC Vive Pro 2 is a commercially available system used mainly for VR applications. The starter kit consists of a headset, two controllers, and two lighthouses. The lighthouses serve as the reference for the controllers and headsets. The lighthouse sends out both a blinking IR light, as well as tracking laser beams across their field of view. The controllers and headset receive the IR blink to start counting, after which the controllers and headset wait for the laser to hit them on one of their sensors, see the indentations in **Fout! Verwijzingsbron niet gevonden.**. By recording the time at which the laser hits the controller/headset after synchronization, the lighthouse can calculate where the object is inside the tracked area. This synchronization happens at a rate of around 60 Hz, and it is also used to correct for drift of the internal IMU of the controllers/headsets, which operates at a much faster rate of 500 Hz. The HTC Vive trackers have the same positional tracking as the controllers/headset and are normally used to bring parts of the wearer's body to the virtual environment, for example, forearms or thighs and shanks. The reported accuracy of the lighthouse system is in the range of a few cm and around one degree for translation and rotation respectively [32], at a sampling rate of around 100 Hz.
The translation and orientation of each tracker are expressed regarding a global reference frame, which the Vive creates when the room and camera trackers are calibrated. Each tracker has its own frame, as specified in the manual, the axes of which can be seen in Figure 15.

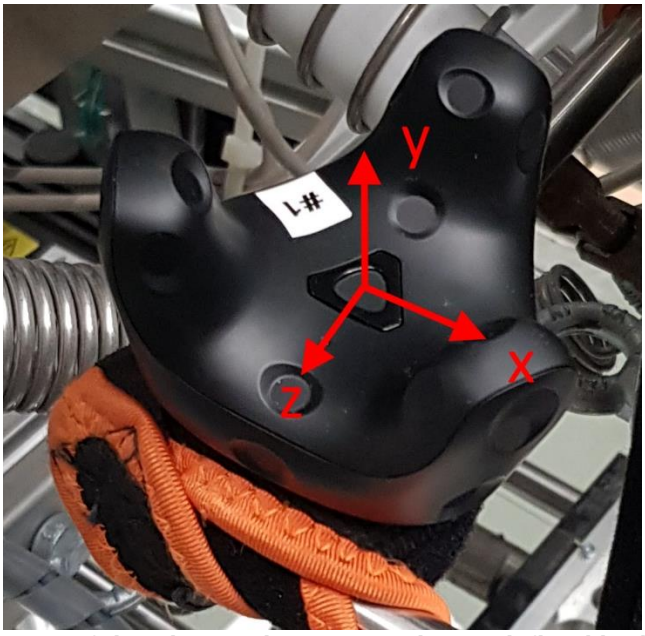

Figure 15: Axes of the Vive tracker, x, y, and z, as defined in the manual.

Steam VR (Valve, USA) was used to manage the different HTC Vive devices and to set up the basic virtual environment. Data recording was done in Unity (Unity Software Inc., USA). A plugin can connect the virtual environment of Steam VR to that of Unity. In Unity, custom plugins can be used to record positional and orientational data of any object in the environment, whether virtual or real. The orientational data can be recorded in both quaternions and Euler angles, both in relation to the aforementioned global reference frame

(GRF) created by Steam VR (Figure 16). Positional data of all the trackers can be recorded in the GRF.

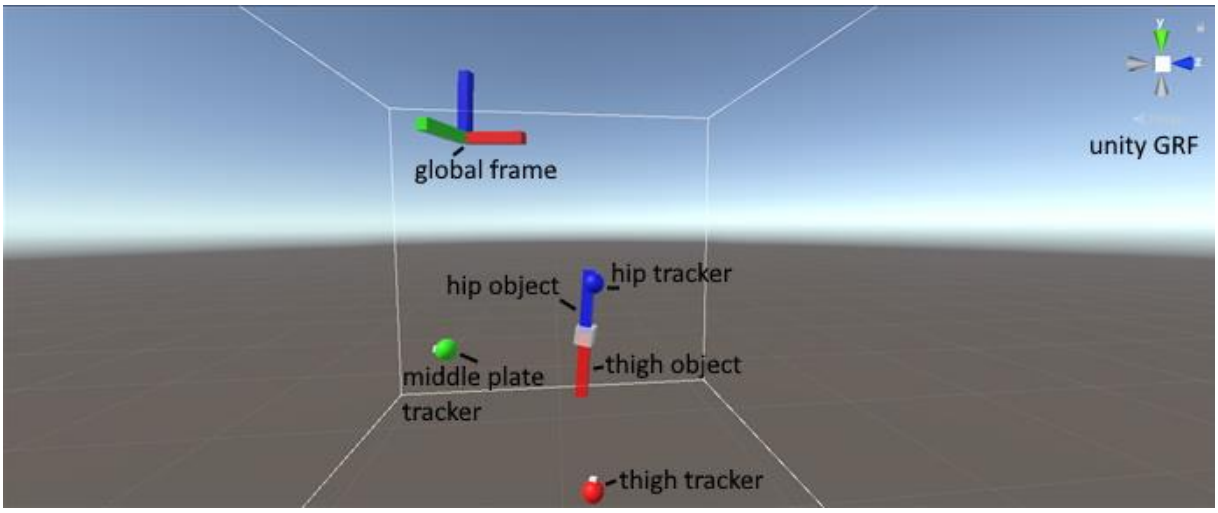

Figure 16: The Unity environment with the middle plate tracker (green) and the global frame tied to it, the thigh tracker (red sphere) and the orientationally offset virtual object thigh object (red beam), as well as the hip tracker (blue ball) and it's virtual object hip object (blue beam). Also included is the Unity GRF.

For the experiment, three trackers were used:

1. Tracker 1 on the thigh of the Lokomat
2. Tracker 2 on the pelvis plate of the Lokomat
3. Tracker 3 on the middle plate of the Lokomat

Tracker 2 and Tracker 3 can be used to find the 6 DOFs of the pelvis in relation to the middle plate. For the position of the pelvis plate, one can simply subtract the position of tracker 1 from tracker 2, resulting in a vector pointing from tracker 1 to tracker 2. Tracker 1 can be placed in such a way that it best coincides with the global frame as described in the kinematics calculation, see the global frame of Figure 10.

Using the recorded Euler angles between the GRF and tracker 1 and tracker 2, the quaternions between tracker 2 and tracker 3 can be calculated using:

$$^{2}\boldsymbol{q}_{3} = {}^{2}\boldsymbol{q}_{GRF}\ {}^{3}\boldsymbol{q}_{GRF}{}^{-1} \tag{15}$$

With $^{2}\boldsymbol{q}_{3}$ the quaternions from frame 2 to frame 3, $^{2}\boldsymbol{q}_{GRF}$ the rotation matrix from the GRF to frame 2 and $^{3}\boldsymbol{q}_{GRF}{}^{-1}$ the conjugated quaternions from frame 3 to the GRF. Using the recorded quaternions angles $^{2}\boldsymbol{q}_{GRF}$ and $^{3}\boldsymbol{q}_{GRF}{}^{-1}$ can be constructed. From quaternions $^{2}\boldsymbol{q}_{3}$, the Euler angles from frame 2 to frame 3 can be calculated using the Matlab quat2eul command, in other words, the orientation of the pelvis plate in relation to the middle plate.

Using tracker 2 and tracker 3, the Euler angles between the thigh and pelvis can be calculated in a similar. These will contain the adduction and flexion angles required for the validation of the kinematics calculation.

To ensure the Vive trackers are tracking the motion correctly, a calibration sequence is performed. Because of the geometry of the Lokomat orthosis, the trackers cannot be placed so that their axes are aligned desirably. Preferably, the trackers would be placed onto the device so that the Euler angles match the adduction/flexion angles that are needed for validation. Furthermore, it can be hard to align the axes of the tracker with the device itself, if done by eye. For calibration, the Lokomat is set in a neutral position, meaning flexion adduction and exo-rotation at 0. This is done using a level to assure that both pelvis plate

and orthosis are in the correct orientation. At this point, the recorded quaternions from the GRF to the trackers can be measured and treated as an initial offset. Another strategy would be to place two virtual bodies in the virtual environment that are orientated the same way, just like the physical device. These virtual bodies can then be rigidly attached to the tracker in unity, so they rotate along with the tracker. The Euler angles of these virtual bodies can then also be recorded, to obtain the Euler angles between bodies without the initial offset due to inconvenient tracker placement. Both calibration strategies were used at once. Once this calibration has been performed, the setup can be used for multiple experiments as long as the Vive lighthouses are not disturbed.

4.3 Experimental procedure

Now that the recording procedures for the Lokomat and the HTC Vive have been described, the plan for the three experiments can be described. The setups for both experiments were the same when it comes to the Lokomat and the HTC Vive. The actuators of the Lokomat were not be used to move the orthosis, nor was the treadmill. The trackers were be placed on the pelvis plate and right thigh and middle plate. Due to the symmetry of the design recording, both legs are redundant. The trackers were recorded by two lighthouses, about two meters from the trackers and the device.

For experiment one, the Lokomat was moved around by hand, with no one wearing the orthosis. The goal of this experiment was to trace the ROM when it comes to the linear actuators, to achieve maximum and minimum flexion and adduction. Achieving maximum flexion/adduction could lead to loss of balance if the exoskeleton is worn, hence it was done by hand. The movement started from a neutral position (0 flexion or abduction), see Figure 17.

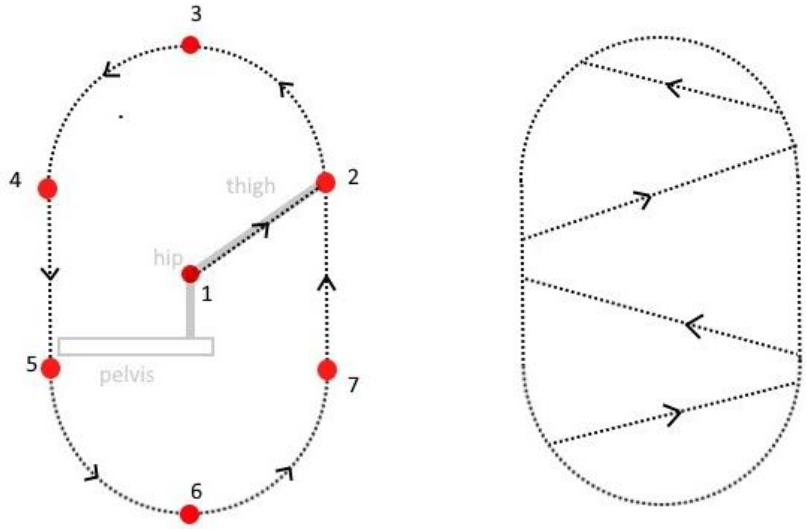

Figure 17: Top view of the movement pattern of the first experiment. On the LEFT is the initial tracing of the ROM, whilst the RIGHT shows an example of the zigzag pattern performed after tracing. Red dots indicate the position of the knee, with 1 being the neutral position, 2 maximum abduction of the hip, 3 maximum flexion, 4 and 5 maximum adduction, 6 maximum extension, and 7 maximum abduction.

From this starting position (1), the thigh was moved to maximum abduction. Following this, the orthosis was be moved so that the hip is flexing, whilst at the same time remaining fully abducted. After one of the actuators reaches its limit (2), the orthosis was pulled into maximum flexion (3). Then the device was pulled into maximum adduction (4) after which it was extended until one of the actuators reached its limit again (5). Continuing, the orthosis was put into maximum extension (6), followed by maximum abduction (7). After this initial tracing of the ROM, the remaining time was being used to move the thigh orthosis around in

a zigzag pattern, moving from the adduction to abduction whilst flexing and extending. During the motion the pelvis plate was left suspended on its springs, free to move around.
The other two experiments involved a person wearing the orthosis. This is the situation in which the kinematics are to be used eventually, hence it is important to test the accuracy of the calculation when applied to human gait. For experiment two, the wearer was lifted slightly off of the ground using the bodyweight support crane, allowing them to freely move around in the air without having to make use of the treadmill. Whilst suspended in the air the subject then attempted a walking motion.
The third experiment had the subject being supported by the BWS, without their feet leaving the ground. Instead, the goal will be to again simulate a walking motion, with just the right leg, whilst dragging the feet across the ground instead of having them suspended in the air. This has the benefit of still providing the wearer of the orthosis with some support on the stance leg.
To do these experiments, the modifications made to the Lokomat had to be assessed for safety. As the actuators will not be powered during the experiments, the main safety concerns are the electrical wiring of the modifications. For this reason, a schematic has been made of the modification, which can be found in Appendix C. With this electrical scheme, the modified Lokomat passed the safety inspection for this experiment.

5 Results

In the results section, the flexion and adduction values of the kinematic calculation, as well as those of the Vive tracker measurement are compared against one another. For each experiment, this comparison is done via a plot of the flexion and adduction angles of both methods, and through the root mean square error between each method.

5.1 Experiment one

The first experiment is the trace of the linear actuator ROM.

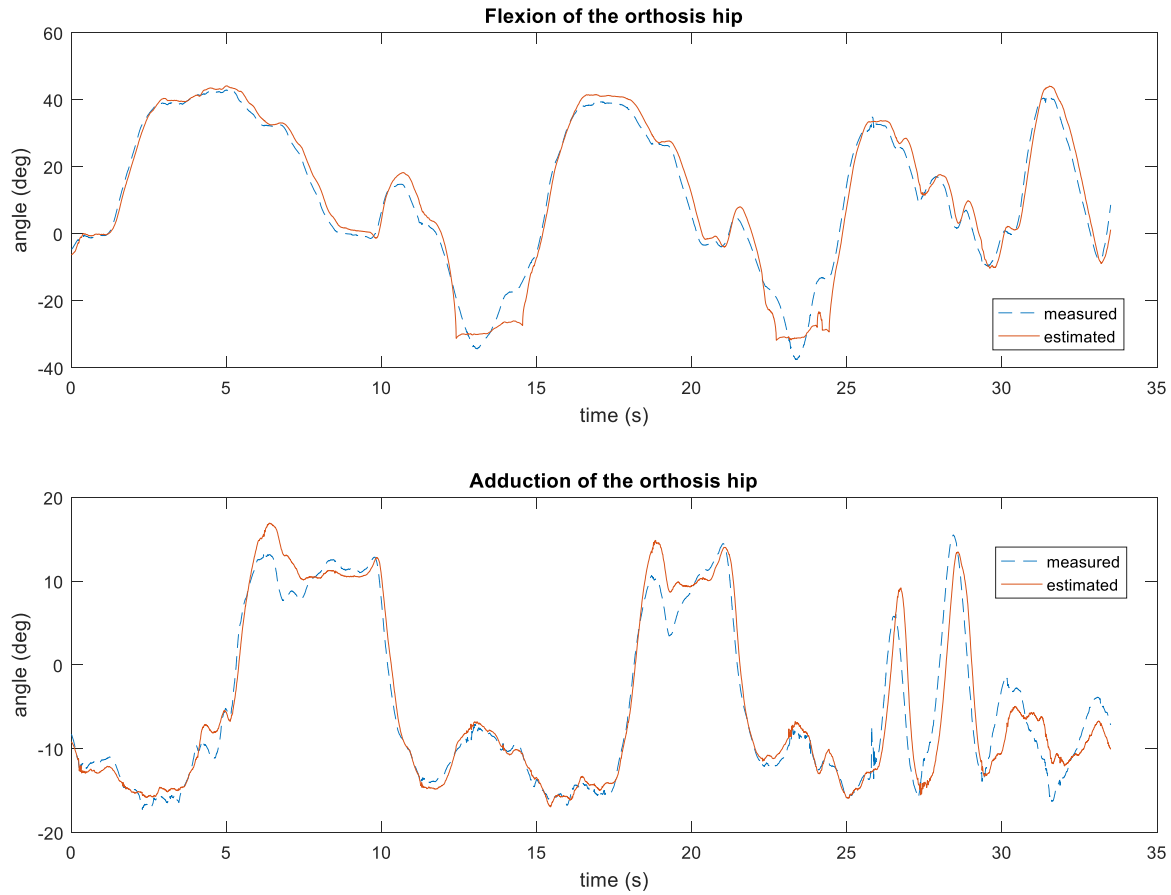

Figure 18: Time vs angle plot of the orthosis hip flexion (above) and adduction (below), for the first experiment. The orange solid line is the corresponding angle as estimated by the kinematics, whilst the blue dashed line represents the actual angle measured by the Vive system.

The orthosis flexion of the kinematics has a very similar shape to that of the measured Vive angles. The only major difference is the flat section at minimum flexion for the estimated flexion angle.

The adduction angles have a less similar shape. Mainly at maximum and minimum adduction, the kinematics remain mostly flat, whereas the measured angles exhibit some additional periodic movements.

5.2 Experiment two

The next experiment involves a subject wearing the Lokomat whilst suspended, trying to make a walking motion.

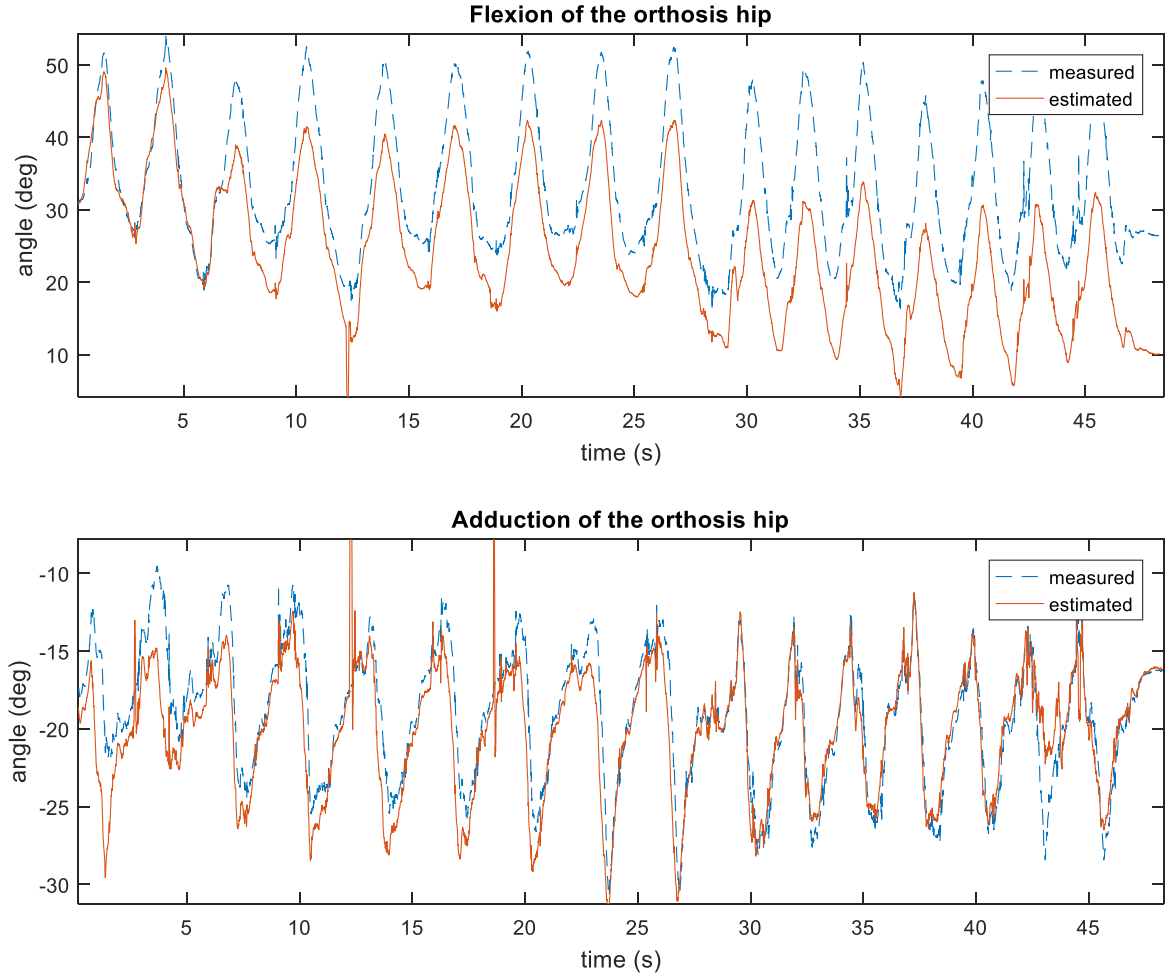

Figure 19: time vs angle plot of the orthosis hip flexion (above) and adduction (below), for the second experiment. The orange solid line is the corresponding angle as calculated by the kinematics, whilst the blue dashed line represents the angle measured by the Vive system.

The flexion graph again has an offset between the kinematics values and the measured values, which is increasing. Timewise, and amplitude-wise, the maxima and minima are very similar between the two. The walking motion is consistent but does not resemble a normal gait. The adduction data matches quite well, however, the estimated values are more jagged. Both adduction and flexion graphs contain outlying peaks in the kinematics data, around 12.5 seconds and 18 seconds. In Appendix B, the same graphs of experiments two and three are presented, with the drift removed. The drift has been removed using the Matlab detrend command.

5.3 Experiment three

Experiment three involves the participant holding their left foot on the ground whilst simulating gait with their right leg, dragging their feet over the ground.

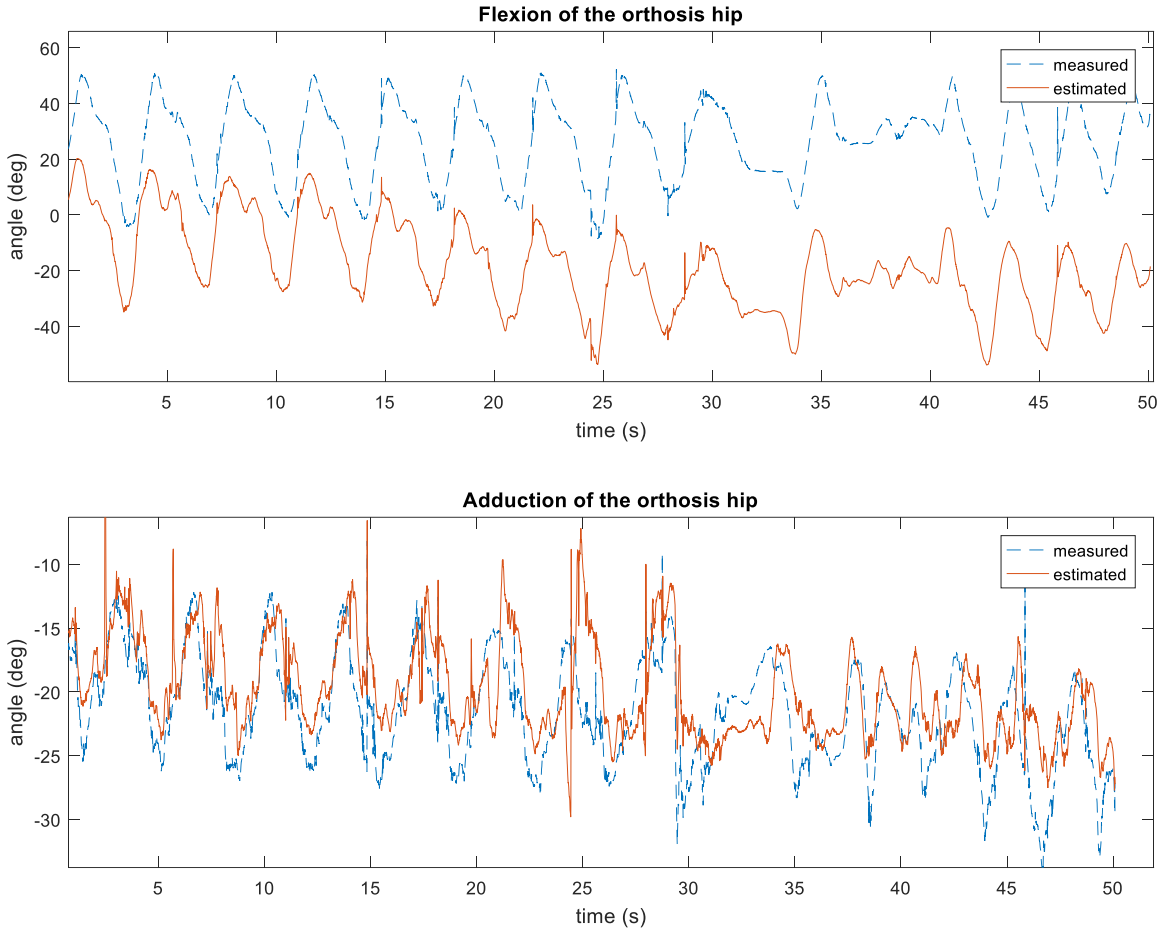

Figure 10: Time vs angle plot of the orthosis hip flexion (above) and adduction (below), for the third experiment. The orange solid line is the corresponding angle as calculated by the kinematics, whilst the blue dashed line represents the angle measured by the Vive system.

The flexion data has a severe vertical offset, although the shape of the graph is very similar. The timing and amplitude of the peaks match very well. For the adduction, both measured and estimated graphs are very jagged, with the estimated graph having outlying peaks at multiple points.

Featured in Table 2 is the Root Mean Square Error (RMSE) of the flexion and adduction angles for all three experiments. To give more context to the RMSE, there is also a reported ratio between the RMSE and the average ROM of each joint angle for normal human gait. The ROM for normal human gait is assumed to be 50 degrees for flexion/extension and 17 for abduction/adduction [33]. Asterisks represent the detrended version of the data.

	RMSE flexion (deg)	$\frac{\text{RMSE}}{\text{ROM}}$ (%)	RMSE adduction (deg)	$\frac{\text{RMSE}}{\text{ROM}}$ (%)
Manual ROM trace	3.18	6.36	1.892	11.1
Suspended	9.921 / 2.72*	19.82 / 5.44*	2.481	14.6
Grounded	45.74 / 7.91*	91.53 / 7.92	3.86	22.7

Table 2: RMSE of the adduction and flexion angles for all three experiments, as well as the ratio between the RMSE and the normal human gait ROM of each joint angle. Asterisks represent the detrended version of the data.

6 Discussion

6.1 Experiment one

There is a small offset between the measured data from the Vive and the kinematics calculation (Figure 18). This difference can be explained by an error in the measurement of some of the components of the Lokomat. There were no CAD files available of the machine, so for example the distance from the actuator joint to the middle plate tracker was measured using a tape measure. Not all distances are easily measurable, hence some inaccuracies may lead to consistent offsets in the angles calculated using the kinematics.
The other main issue with performance is at minimum flexion. The kinematics estimation does not go below -28 degrees flexion, whereas the measured angles reach -37 degrees flexion at their minima. The flat part in the estimated angles indicates that the kinematics calculations stopped intersecting beyond these flexion values, leading to the flat area. This could be explained by the aforementioned errors in the measured parameters of the calculation. These offsets would lead to the hip and actuator circles being too far apart in extreme situations.
The adduction data matches quite well, but at maximum adduction, there is a difference in shape between the graphs. The kinematics calculation has a higher overshoot and has a less deep valley afterward compared to the measured data. This data could be explained by small offsets in the virtually calibrated global frame. The calibration of this virtual object was not perfect, and small offsets in these angles could lead to other angles interfering with the graph of the estimated and measured angles.
Looking at the minima and maxima of the data, maximum flexion and extension are somewhere between 43.1 and -34.5 degrees according to measured data, with abduction/adduction values varying between -17.7 and -14.2 degrees (measured data). These values could all be seen as the limits of human gait with an extra 10-5 degrees of ROM [34].

6.2 Experiment two and three

In the second and third experiments, the flexion graphs seemed to diverge. The estimated flexion got lower and lower, getting worse from experiment 2 to experiment 3. At the end of experiment 2, the gap is around 12 degrees. Starting in experiment one, the gap has increased to 25 degrees increasing to over 50 at the end of the dataset. Despite this increased gap, the amplitude and period of the peaks remain similar between datasets. The fact that there is drift can be demonstrated by the flexion graphs of experiment three, where the measured data exceeds the upper limit of flexion, as found in experiment 1, whilst the estimated data exceeds the lower limit of flexion. The adduction graphs in both cases exceed the lower limit of adduction as found in experiment one. This difference cannot be explained through the increased tilt of the pelvis, as the variation in pelvis tilt was not found to be more than +2/-2 degrees for normal human gait [27]. The drift can be seen in the graphs of the recorded Euler angles for the virtual global reference frame, tied to angle tracker 3. Tracker three should not rotate in relation to the GRF made by unity and neither should the virtual object linked to it, yet the virtual object shows over 100 degrees of rotation in 2 Euler angles for experiment three and 70 degrees of rotation in 2 Euler angles for experiment 2. The drift has been removed using the Matlab detrend command in Appendix B, subtracting the best straight line from the data This was done since the data of human gait is expected to be periodic and should not contain a linear upward or downward trend. Furthermore, because of the many rotations performed in the calculation of the orthosis hip joint angles, it is hard to pinpoint the effect the rotational drift has on the final result, hence a more blind approach like the detrend command was chosen. As seen in Table 2 and Appendix B, the detrended data shows performance similar to that of experiment one.

Both experiment 2 and experiment 3 contain several spikes in the data. These spikes indicate that one or more of the trackers involved in the calculation of the angles lost connection. The algorithm used to detect these spikes was based on large spikes in the positional data of the trackers, but there are more spikes in the orientational data than in the positional data, leading to some spikes remaining. The spikes in orientational data are smaller and harder to detect, as they are less exaggerated compared to the positional spikes, however, they can still lead to significant spikes in the end result. To remove the spikes a low pass filter could be used, however, this could also remove other high-frequency changes in orientation that are part of the signal.

6.3 Recommendations for future research

The main recommendations given the results of the experiment are:

1. Use the original Lokomat sensors for determining the pelvis position and orientation, This saves having to synchronize the Lokomat and unity dataset until the final comparison. Furthermore, the Lokomat data should not suffer from as much drift as the Vive data, since its sensors are tightly attached to the orthosis.
2. Make better sensor mounts for the Vive trackers, to prevent drift. These could be 3D-printed.
3. Make more accurate measurements of the orthosis components, to prevent offsets in the kinematics data
4. Do the experiments with a working treadmill for more natural gait patterns

7 Conclusion

In this thesis, a kinematics calculation has been proposed for calculating the hip angles of an end-effector-based orthosis. Using eight independent generalized coordinates as input, two actuator extensions and the six degrees of freedom of the pelvis plate, the adduction and flexion angles of the orthosis hip can be calculated. This method is mainly based on the intersection of circles and spheres for representing non-measured angles of joints within the mechanism. This calculation was validated using an HTC Vive 2.0 VR system, used for motion capture of the adduction and flexion angles. Three experiments were performed to validate these angles, the first involved moving the orthosis around by hand, and the second and third with a person wearing the orthosis under different circumstances. When looking at the first experiment, the kinematics perform quite well, with an RMSE of only 3.18 degrees and 1.89 degrees for flexion and adduction respectively. Given this experiment traces the entire ROM, this performance is quite good. Later experiments suffered from major drift in the Vive trackers. This lead to a major offset in the flexion graph. Detrended data still shows good performance, especially for flexion. Using the original sensor of the Lokomat for finding the Euler angles should eliminate this drift and is expected to make major improvements to performance. Despite the tracker issues in later experiments, the first experiment and the similarity in graph shapes in later experiments point toward the proposed kinematics calculation being correct and useable.

Bibliography

[1] E. J. Benjamin *et al.*, *Heart Disease and Stroke Statistics-2019 Update: A Report From the American Heart Association*, vol. 139, no. 10. 2019.

[2] P. W. Duncan *et al.*, “Management of Adult Stroke Rehabilitation Care: a clinical practice guideline.,” *Stroke.*, 2005, doi: 10.1161/01.STR.0000180861.54180.FF.

[3] H. Barbeau, M. Wainberg, and L. Finch, “Description and application of a system for locomotor rehabilitation,” *Med. Biol. Eng. Comput.*, 1987, doi: 10.1007/BF02447435.

[4] R. Riener, L. Lünenburger, I. C. Maier, G. Colombo, and V. Dietz, “Locomotor training in subjects with sensori-motor deficits: An overview of the robotic gait orthosis Lokomat,” *J. Healthc. Eng.*, vol. 1, no. 2, pp. 197–216, 2010, doi: 10.1260/2040-2295.1.2.197.

[5] P. R. Lucareli, M. O. Lima, F. P. S. Lima, J. G. De Almeida, G. C. Brech, and J. M. D’Andréa Greve, “Gait analysis following treadmill training with body weight support versus conventional physical therapy: A prospective randomized controlled single blind study,” *Spinal Cord*, vol. 49, no. 9, pp. 1001–1007, 2011, doi: 10.1038/sc.2011.37.

[6] S. C. Cramer and J. D. Riley, “Neuroplasticity and brain repair after stroke,” *Current Opinion in Neurology*. 2008, doi: 10.1097/WCO.0b013e3282f36cb6.

[7] G. Martino, “How the brain repairs itself: New therapeutic strategies in inflammatory and degenerative CNS disorders,” *Lancet Neurology*. 2004, doi: 10.1016/S1474-4422(04)00771-9.

[8] R. Riener, L. Lünenburger, S. Jezernik, M. Anderschitz, G. Colombo, and V. Dietz, “Patient-cooperative strategies for robot-aided treadmill training: First experimental results,” *IEEE Trans. Neural Syst. Rehabil. Eng.*, vol. 13, no. 3, pp. 380–394, 2005, doi: 10.1109/TNSRE.2005.848628.

[9] L. Marchal-Crespo and R. Riener, *Robot-assisted gait training*. Elsevier Ltd., 2018.

[10] J. Mehrholz, S. Thomas, C. Werner, J. Kugler, M. Pohl, and B. Elsner, “Electromechanical-assisted training for walking after stroke,” *Cochrane Database of Systematic Reviews*. 2017, doi: 10.1002/14651858.CD006185.pub4.

[11] M. Lotze, C. Braun, N. Birbaumer, S. Anders, and L. G. Cohen, “Motor learning elicited by voluntary drive,” *Brain*, vol. 126, no. 4, pp. 866–872, 2003, doi: 10.1093/brain/awg079.

[12] D. S. Reisman, H. McLean, J. Keller, K. A. Danks, and A. J. Bastian, “Repeated split-belt treadmill training improves poststroke step length asymmetry,” *Neurorehabil. Neural Repair*, vol. 27, no. 5, pp. 460–468, 2013, doi: 10.1177/1545968312474118.

[13] J. L. Emken and D. J. Reinkensmeyer, “Robot-enhanced motor learning: Accelerating internal model formation during locomotion by transient dynamic amplification,” *IEEE Trans. Neural Syst. Rehabil. Eng.*, vol. 13, no. 1, pp. 33–39, 2005, doi: 10.1109/TNSRE.2004.843173.

[14] S. Jezernik, R. Scha, G. Colombo, and M. Morari, “Adaptive robotic rehabilitation of locomotion : a clinical study in spinally injured individuals,” *Spinal Cord*, no. 41, pp. 657–666, 2003, doi: 10.1038/sj.sc.3101518.

[15] B. A. English and A. M. Howard, “The Effects of Auditory and Visual Cues on Timing Synchronicity for Robotic Rehabilitation,” pp. 682–688, 2017.

[16] T. Klarner, J. S. Blouin, M. G. Carpenter, and T. Lam, “Contributions to enhanced activity in rectus femoris in response to Lokomat-applied resistance,” *Exp. Brain Res.*, vol. 225, no. 1, pp. 1–10, 2013, doi: 10.1007/s00221-012-3345-8.

[17] R. S. Calabrò *et al.*, “Robotic gait training in multiple sclerosis rehabilitation: Can virtual reality make the difference? Findings from a randomized controlled trial,” *J. Neurol. Sci.*, vol. 377, pp. 25–30, 2017, doi: 10.1016/j.jns.2017.03.047.

[18] P. Tsangaridis, D. Obwegeser, S. Maggioni, R. Riener, and L. Marchal-Crespo, “Visual and Haptic Error Modulating Controllers for Robotic Gait Training,” in *Proceedings of the IEEE RAS and EMBS International Conference on Biomedical Robotics and*

Biomechatronics, 2018, vol. 2018-Augus, pp. 1050–1055, doi: 10.1109/BIOROB.2018.8488011.
[19] R. S. Calabrò *et al.*, “The role of virtual reality in improving motor performance as revealed by EEG: a randomized clinical trial,” *J. Neuroeng. Rehabil.*, vol. 14, no. 1, pp. 1–16, 2017, doi: 10.1186/s12984-017-0268-4.
[20] L. Marchal-Crespo, P. Tsangaridis, D. Obwegeser, S. Maggioni, and R. Riener, “Haptic error modulation outperforms visual error amplification when learning a modified gait pattern,” *Front. Neurosci.*, vol. 13, no. FEB, pp. 1–24, 2019, doi: 10.3389/fnins.2019.00061.
[21] M. Wellner, M. Guidali, J. Von Zitzewitz, and R. Riener, “Using a robotic gait orthosis as haptic display - A perception-based optimization approach,” *2007 IEEE 10th Int. Conf. Rehabil. Robot. ICORR’07*, vol. 00, no. c, pp. 81–88, 2007, doi: 10.1109/ICORR.2007.4428410.
[22] V. A. D. Cai, A. Ibanez, C. Granata, V. T. Nguyen, and M. T. Nguyen, “Transparency enhancement for an active knee orthosis by a constraint-free mechanical design and a gait phase detection based predictive control,” *Meccanica*, vol. 52, no. 3, pp. 729–748, 2017, doi: 10.1007/s11012-016-0575-z.
[23] T. Proietti, V. Crocher, A. Roby-Brami, and N. Jarrasse, “Upper-limb robotic exoskeletons for neurorehabilitation: A review on control strategies,” *IEEE Rev. Biomed. Eng.*, vol. 9, pp. 4–14, 2016, doi: 10.1109/RBME.2016.2552201.
[24] H. Kim, L. M. Miller, Z. Li, J. R. Roldan, and J. Rosen, “Admittance control of an upper limb exoskeleton - Reduction of energy exchange,” in *Proceedings of the Annual International Conference of the IEEE Engineering in Medicine and Biology Society, EMBS*, 2012, pp. 6467–6470, doi: 10.1109/EMBC.2012.6347475.
[25] J. F. Veneman, J. Menger, E. H. F. van Asseldonk, F. C. T. van der Helm, and H. van der Kooij, “Fixating the pelvis in the horizontal plane affects gait characteristics,” *Gait Posture*, vol. 28, no. 1, pp. 157–163, 2008, doi: 10.1016/j.gaitpost.2007.11.008.
[26] D. Wyss, “Enabling Balance Training in Robot-Assisted Gait Rehabilitation,” ETH Zurich, 2019.
[27] D. Wyss, A. Pennycott, V. Bartenbach, R. Riener, and H. Vallery, “A MUltidimensional Compliant Decoupled Actuator (MUCDA) for Pelvic Support During Gait,” *IEEE/ASME Trans. Mechatronics*, vol. 24, no. 1, pp. 164–174, 2019, doi: 10.1109/TMECH.2018.2878289.
[28] S. Jezernik, A. Pfister, H. Frueh, G. Colombo, and M. Morari, “Robotic orthosis Lokomat: its use in the rehabilitation of locomotion and in the development of the biology-based neural controller,” *7th Annu. Conf. Int. Funct. Electr. Stimul. Soc.*, no. January, p. 102, 2002, [Online]. Available: http://ifess.org/proceedings/IFESS2002/IFESS2002_102_Jezernik.pdf.
[29] J. Jiang, W. Li, and K. M. Lee, “A Novel Pantographic Exoskeleton Based Collocated Joint Design with Application for Early Stroke Rehabilitation,” *IEEE/ASME Trans. Mechatronics*, vol. 25, no. 4, pp. 1922–1932, 2020, doi: 10.1109/TMECH.2020.2992993.
[30] P. Bourke, “Circles and spheres,” 1997. http://paulbourke.net/geometry/circlesphere/ (accessed Jun. 28, 2021).
[31] C. A. Sharp, H. Davies, M. Davie, and M. J. Haddaway, “ISB recommendation on definitions of joint coordinate system of various joints for the reporting of human joint motion—part I: ankle, hip, and spine,” *J. Biomech.*, vol. 40, no. 5, pp. 256–257, 2002, doi: 10.1038/sj.sc.3101287.
[32] D. C. Niehorster, L. Li, and M. Lappe, “The accuracy and precision of position and orientation tracking in the HTC vive virtual reality system for scientific research,” *Iperception.*, vol. 8, no. 3, pp. 1–23, 2017, doi: 10.1177/2041669517708205.
[33] H. Kainz *et al.*, “Reliability of four models for clinical gait analysis,” *Gait Posture*, vol. 54, no. November 2016, pp. 325–331, 2017, doi: 10.1016/j.gaitpost.2017.04.001.
[34] D. Winter, *THE BIOMECHANICS AND MOTOR CONTROL OF HUMAN GAIT: NORMAL, ELDERLY AND PATHOLOGICAL*, 2nd ed., vol. 2. 1991.

Appendix A: Intersection of circles

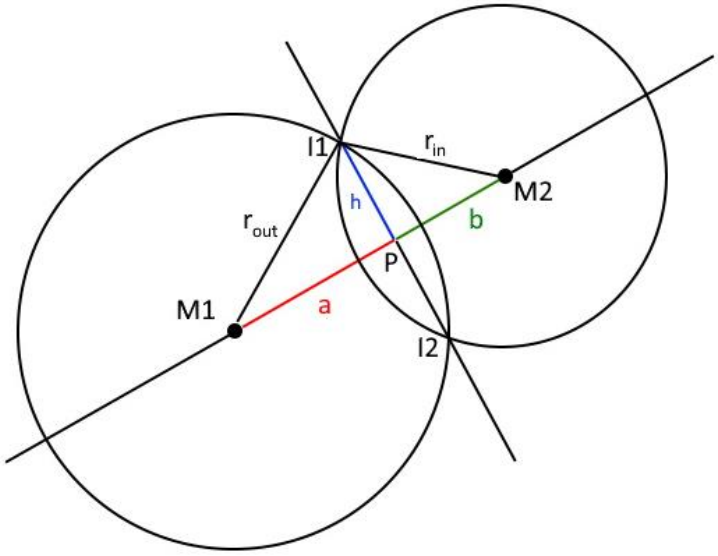

Figure 11: Intersection calculation for two spheres in the same plane, with M1 and M2 the centers of the circles with radii r_{out} and r_{in} respectively. Point P is a point on the vector from M1 to M2 used to make two right triangles. The right triangles are both made using the intersection point of the circle I1. a, b and h are segment lengths of these triangles.

Given two circles with centers $\mathbf{M_1}$ and $\mathbf{M_2}$ and radii r_{out} and r_{in} the intersection points of these circles, $\mathbf{I_1}$ and $\mathbf{I_2}$ can be found using the following derivation taken from [30]:

$$d = \|\boldsymbol{M_1} - \boldsymbol{M_2}\|$$

Using triangles $\mathbf{M_1I_1P}$ and $\mathbf{M_2I_1P}$ and the Pythagorean theorem:

$$r_{out}{}^2 = a^2 + h^2$$

$$r_{in}{}^2 = b^2 + h^2$$

Which can be solved for a by substituting and using

$$d = a + b$$

Resulting in:

$$a = \frac{(r_{out}{}^2 - r_{in}{}^2 + d^2)}{2d}$$

This can be used to find point **P**:

$$\boldsymbol{P} = \boldsymbol{M_1} + \frac{a}{d}(\boldsymbol{M_2} - \boldsymbol{M_1})$$

From point **P**, the x and y coordinates of $\mathbf{I_1}$ and $\mathbf{I_2}$ can be found through:

$$x_I = x_P + - \frac{h(y_{M2} - y_{M2})}{d}$$

$$y_I = y_P - + \frac{h(x_{M2} - x_{M2})}{d}$$

With the + - signs determining whether it is $\mathbf{l_2}$ or $\mathbf{l_1}$

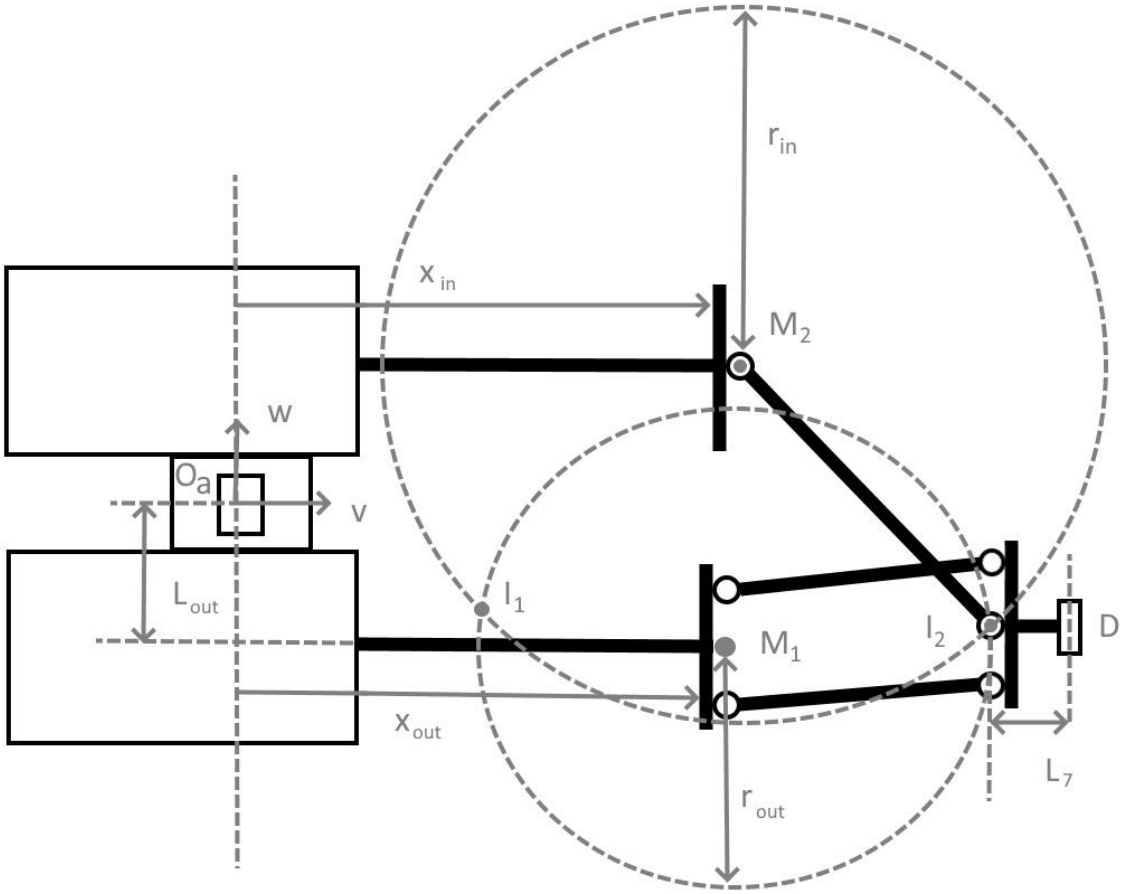

Figure 12: Two-dimensional drawing of the thigh actuation linkages. The frame O_a is attached to body 1 and centered at point O_a, with axes v and w. The x_{in} and x_{out} represent the extension of the actuators and are the two independent generalized coordinates. L_{out} is the distance from O_a to the actuator slider in the w-axis direction. The circles, with middle points M_1 and M_2 and radii, r_{in}, and r_{out} represent the range of motion of the endpoint of the inner and outer linkages respectively. The circles intersect at points l_1 and l_2. L_7 is the distance from point l_2 to joint D.

The goal of the intersection calculation is to find the position of point **D** in the drawing above, as a function of the generalized coordinates x_{in} and x_{out}. This means that the points $\mathbf{M_1}$ and $\mathbf{M_2}$ must be described in the body-fixed frame at point **O**:

$$\begin{aligned} v_{M2} &= x_{in} \\ w_{M2} &= L_{out} \\ v_{M1} &= x_{out} \\ w_{M1} &= -L_{out} \end{aligned}$$

With $\mathbf{M_1}$, $\mathbf{M_2}$, r_{out} and r_{in}, known $\mathbf{l_1}$ and $\mathbf{l_2}$ can be calculated. In order to find out whether the actual device is in configuration 1 or 2, an additional set of constraints can be used:

$$v_I \geq v_{M2} \quad \wedge \quad v_I \geq v_{M1}$$

These constraints state that the v_I, v coordinate of an intersection point, cannot be smaller than the v coordinate of the center of one of the circles. This is because the plate on the actuator slider blocks the motion of the slider, limiting it to a ROM of a semicircle. In the figure above, $\mathbf{I_1}$ breaks this constraint, thus $\mathbf{I_2}$ is the actual location of the linkage endpoints in the physical device. Applying this in the circle intersection calculation, we know the lower value of x_I will always break this constraint before the higher value, so the correct value is:

$$v_I = v_P + \frac{h(w_{M2} - w_{M2})}{d}$$

$$w_I = w_P - \frac{h(v_{M2} - v_{M2})}{d}$$

Due to the parallel constraint, **D** can always be found from $\mathbf{I_2}$ using:

$$v_D = v_{I2} + L_7$$
$$w_D = w_{I2}$$

Appendix B: Detrended results

Experiment two:

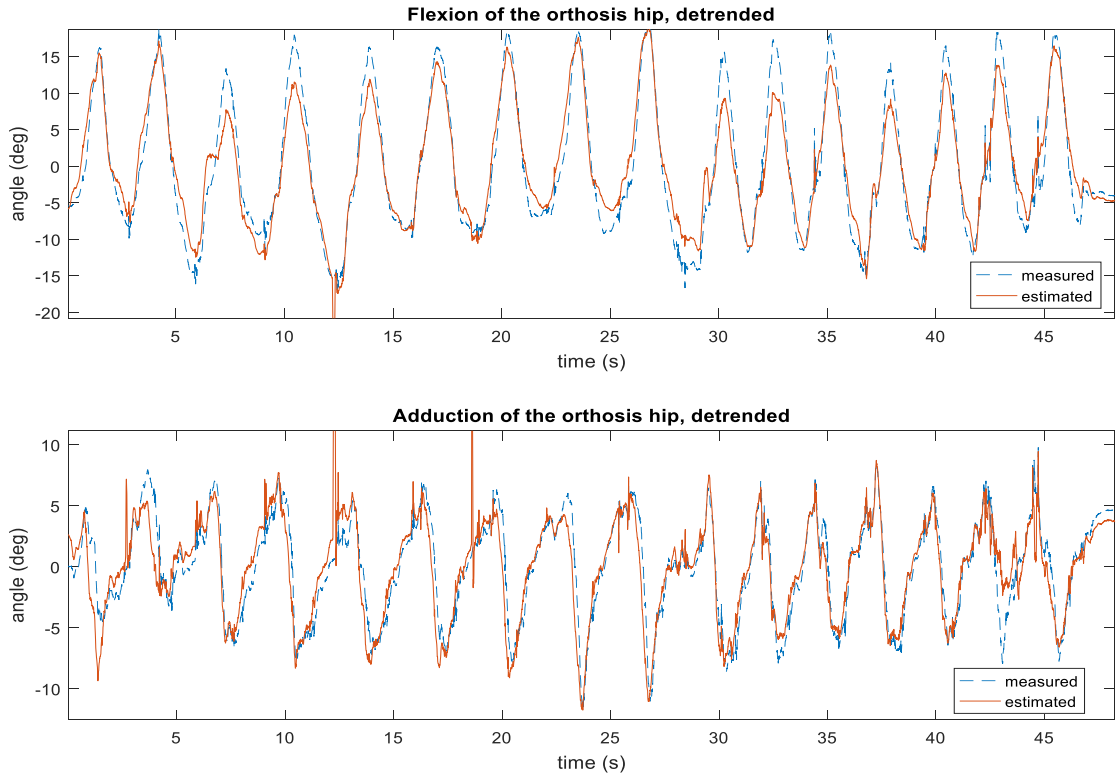

Figure 13: Time vs angle plot of the detrended orthosis hip flexion (above) and adduction (below), for the second experiment. The orange solid line is the corresponding angle as calculated by the kinematics, whilst the blue dashed line represents the angle measured by the Vive system

Experiment three:

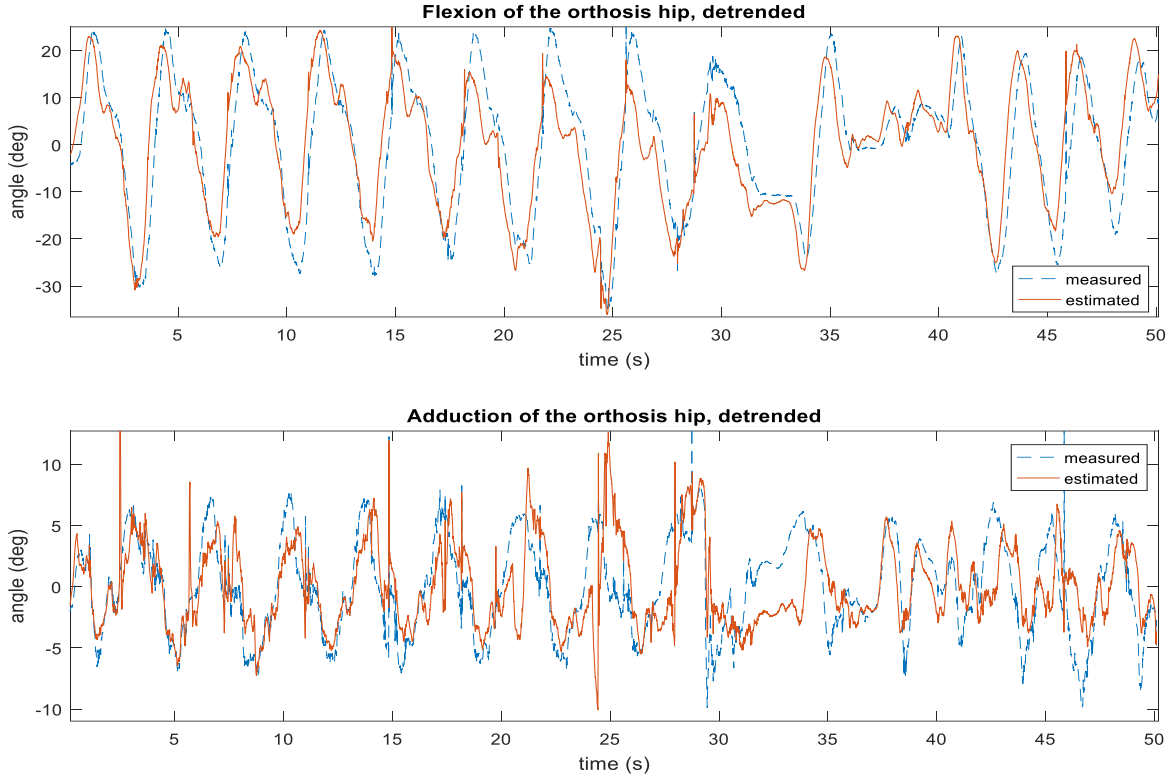

Figure 14: Time vs angle plot of the detrended orthosis hip flexion (above) and adduction (below), for the third experiment. The orange solid line is the corresponding angle as calculated by the kinematics, whilst the blue dashed line represents the angle measured by the Vive system.

Appendix C: Electrical scheme

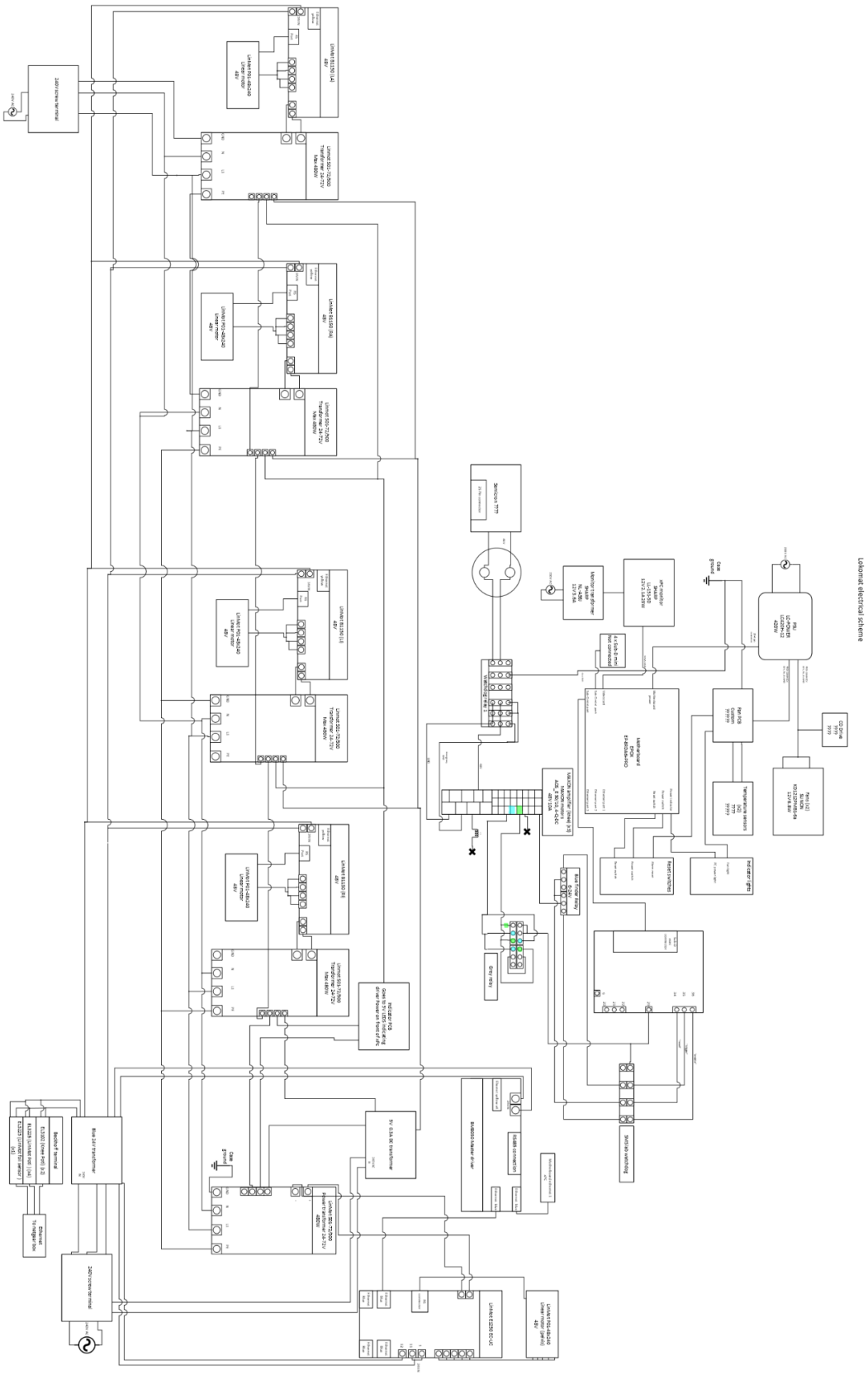

Figure 15: Electrical scheme of the electronics added in the modification